

Phosphorylation at Ser⁷²⁴ of the ER stress sensor IRE1 α governs its activation state and limits ER stress-induced hepatosteatosis

Received for publication, December 9, 2021, and in revised form, April 20, 2022. Published, Papers in Press, April 29, 2022.

<https://doi.org/10.1016/j.jbc.2022.101997>

Yang Li¹ , Shijia Huang¹, Jingsi Wang¹, Jianli Dai² , Jie Cai¹ , Shuai Yan³ , Zhiliang Huang³, Shengqi He¹, Ping Wang³ , Jianmiao Liu⁴, and Yong Liu^{1,*} 

From the ¹Hubei Key Laboratory of Cell Homeostasis, College of Life Sciences, Frontier Science Center for Immunology and Metabolism, and the Institute for Advanced Studies, Wuhan University, Wuhan, China; ²Key Laboratory of Nutrition and Metabolism, Institute for Nutritional Sciences, Shanghai Institutes for Biological Sciences, Chinese Academy of Sciences, Shanghai, China; ³Britton Chance Center for Biomedical Photonics, Wuhan National Laboratory for Optoelectronics-Huazhong University of Science and Technology, Wuhan, Hubei, China; and ⁴Cellular Signaling Laboratory, Key Laboratory of Molecular Biophysics of Ministry of Education, Huazhong University of Science and Technology, Wuhan, China

Edited by Ursula Jakob

Inositol-requiring enzyme 1 (IRE1) is an evolutionarily conserved sensor of endoplasmic reticulum (ER) stress and mediates a key branch of the unfolded protein response in eukaryotic cells. It is an ER-resident transmembrane protein that possesses Ser/Thr protein kinase and endoribonuclease (RNase) activities in its cytoplasmic region. IRE1 is activated through dimerization/oligomerization and autophosphorylation at multiple sites, acting through its RNase activity to restore the functional capacity of the ER. However, it remains poorly defined *in vivo* how the autophosphorylation events of endogenous IRE1 govern its dynamic activation and functional output. Here, we generated a mouse model harboring a S724A knock-in mutation (*Ern1*^{S724A/S724A}) and investigated the importance of phosphorylation at Ser⁷²⁴ within the kinase activation loop of murine IRE1 α . We found that in mouse embryonic fibroblast cells and in primary hepatocytes, S724A mutation resulted in markedly reduced IRE1 α autophosphorylation in parallel with blunted activation of its RNase activity to catalyze X-box binding protein 1 (*Xbp1*) mRNA splicing. Furthermore, ablation of IRE1 α phosphorylation at Ser⁷²⁴ exacerbated ER stress-induced hepatic steatosis in tunicamycin-treated *Ern1*^{S724A/S724A} mice. This was accompanied by significantly decreased hepatic production of spliced XBP1 protein but increased CCAAT-enhancer-binding protein homologous protein (CHOP) level, along with suppressed expression of key metabolic regulators of fatty acid β -oxidation and lipid secretion. These results demonstrate a critical role of phosphorylation at Ser⁷²⁴ of IRE1 α in dynamically controlling its kinase activity, and thus its autophosphorylation state, which is coupled to activation of its RNase activity in counteracting hepatic steatosis under ER stress conditions.

In eukaryotic cells, the endoplasmic reticulum (ER) is a continuous membrane network that performs a variety of crucial functions, including the synthesis, folding, and processing of nearly one-third of the cellular proteome. Excess accumulation of unfolded or misfolded proteins within the ER lumen results in ER stress, triggering the activation of the adaptive cellular response referred to as the unfolded protein response (UPR) (1–3). Three ER-resident transmembrane signal transducers, PKR-like endoplasmic reticulum kinase (PERK), activating transcription factor 6, and inositol-requiring enzyme 1 (IRE1), constitute the three canonical UPR signaling branches to manage ER stress and restore cellular homeostasis (1, 2). A great number of studies have demonstrated the pivotal roles of the UPR pathways in cell fate decisions (4) as well as their implications in many pathological conditions including cancer and metabolic disorders (5–8).

IRE1 is an ancient UPR sensor that is highly conserved from yeast to mammals, including humans (9–11). It possesses the ER luminal domain sensing unfolded/misfolded proteins and the cytoplasmic region with dual Ser/Thr protein kinase and endoribonuclease (RNase) activities mediating its functional outputs (12–14). Upon ER stress, IRE1 RNase is activated through dimerization/oligomerization and transautophosphorylation (15–18), catalyzing the unconventional splicing of the mRNA encoding X-box binding protein 1 (XBP1) to generate a spliced transcriptionally active transcription factor XBP1s (19–21). The IRE1–XBP1 pathway initiates a key UPR gene expression program that enhances the protein folding capacity of the ER and the ER-associated degradation of unfolded/misfolded proteins (4, 14, 22–25). Another effector output of the RNase activity of IRE1 is the degradation of select sets of mRNAs or pre-miRNAs in a process termed “regulated IRE1-dependent decay” (RIDD) (26–30). Emerging lines of evidence have also demonstrated that in mammals, IRE1 α not only has a critical prosurvival role in coping with ER stress but also acts as a multifunctional regulator in response to nutrient stress and metabolic cues (3, 31, 32). A multitude of hormonal, metabolic, and immune signals have been

* For correspondence: Yong Liu, liuyong31279@whu.edu.cn.

Present address for Jianli Dai: Abcam Biotech Co Ltd, Hangzhou 310015, China.

Phosphorylation regulation of IRE1 α activation

shown to instigate the activation of IRE1 α signaling in various metabolic tissues (32), but the precise intracellular mechanisms as well as the molecular signatures with regard to its activation mode and functional output have yet to be fully understood.

Autophosphorylation is a key feature of IRE1 activation in response to ER stress, and its RNase activity is thought to depend upon its kinase activity (33–35). Biophysical structure studies of the cytoplasmic kinase/RNase portion of yeast IRE1 have shown that dimerization (16) or oligomerization assembly (17) may position the kinase domain for trans-autophosphorylation at multiple sites, for example, up to 17 residues based on a mass spectrometry assessment (17). Transautophosphorylation is proposed to promote the nucleotide binding and further facilitate its dimerization or oligomer assembly, leading to intrinsic conformational changes for activating its C-terminal RNase domain for RNA substrate processing (16, 17). Structural characterization of the cytoplasmic domain of dephosphorylated human IRE1 α bound to ADP has revealed a phosphoryl-transfer-competent dimeric face-to-face complex, with the tip of its kinase activation segment between residues 720 and 730 found to be poorly ordered (18). Moreover, phosphorylation of three residues, Ser⁷²⁴, Ser⁷²⁶, and Ser⁷²⁹, within this conserved kinase activation segment in mammalian IRE1 α , has been directly identified from overexpressed cytoplasmic portion of human IRE1 α protein (36), and phosphorylation of these sites can affect its RNase activity for *Xbp1* mRNA splicing as well as RIDD of certain mRNA substrates (36, 37). However, mutational analyses using overexpressed IRE1 α proteins also suggested that phosphorylation of the activation loop is not required for *Xbp1* mRNA splicing/cleavage, and phosphorylation at Ser⁷²⁴ and Ser⁷²⁶, but not Ser⁷²⁹, can exert an enhancing effect upon its RNase activity (36). Interestingly, a recent study showed that phosphorylation at Ser⁷²⁹ of endogenous IRE1 α in B cells or mouse multiple myeloma cells can be robustly and selectively stimulated by lipopolysaccharides and the bacterial subtilase cytotoxin but not by typical ER stressors such as tunicamycin (Tm) (38). In addition, Ser⁷²⁹ phosphorylation was shown to be dispensable for *Xbp1* mRNA splicing activity of IRE1 α in lipopolysaccharide-stimulated B cells, and it might exert a prominent enhancing effect upon its RIDD activity *in vivo*. However, it is unclear whether S729A knock-in mutation can alter the kinase activity of IRE1 α for phosphorylating other sites in response to stress stimuli in B cells (38). Therefore, phosphorylation of individual sites, particularly the three residues within the kinase activation loop of IRE1 α , can respond to distinct stress signals, suggesting that the phosphorylation events serve to govern the activation mode of its RNase for exerting context-specific effector functions.

Despite the recent progress in our understanding of the molecular details *in vitro* with regard to the phosphorylation-activation features of IRE1 α , it remains largely obscure whether phosphorylation within its kinase activation loop is critically implicated in the dynamic regulation of endogenous IRE1 α activation during ER stress *in vivo*. Importantly, phosphorylation at Ser⁷²⁴ has long been widely utilized for monitoring IRE1 α activation in response to a variety of stress signals

under physiological or pathological conditions. Hence, we generated a mouse model (*Ern1*^{S724A/S724A}) possessing the S724A knock-in mutation to abolish phosphorylation at this site and investigated the importance of Ser⁷²⁴ phosphorylation-dependent control of the dynamic activation of IRE1 α protein during typical ER stress and determined its functional impact *in vivo* in the context of ER stress-induced hepatic steatosis.

Results

Generation of the *Ern1*^{S724A/S724A} knock-in mouse model

To determine the functional impact of phosphorylation at Ser⁷²⁴ upon the activation of endogenous IRE1 α *in vivo*, we created a knock-in mutant mouse model, denoted *Ern1*^{S724A/S724A}, in which the Ser⁷²⁴ residue (AGT) was replaced by Ala⁷²⁴ (GCT) within the *Ern1* locus (Fig. 1A). After backcrossing into the genetic background of C57BL/6J mice, *Ern1*^{S724A/S724A} animals were grossly normal, born at normal Mendelian ratios with no overt phenotypic changes in comparison to their *Ern1*^{WT/WT} littermates such as their body weight (Fig. 1B). Using the commercial antibody directed against phospho-IRE1 α at Ser⁷²⁴, we detected robust IRE1 α phosphorylation at this site from primary hepatocytes isolated from WT *Ern1*^{WT/WT} control animals but observed no detectable signals from their *Ern1*^{S724A/S724A} counterparts upon ER stress induced by Tm or thapsigargin (Tg), the two chemical ER stressors (Fig. 1C). This indicates the successful abrogation of IRE1 α phosphorylation at Ser⁷²⁴ within its kinase activation loop in *Ern1*^{S724A/S724A} knock-in mice.

S724A mutation results in lower autophosphorylation of IRE1 α with decreased RNase activation

We then generated immortalized mouse embryonic fibroblast (MEF) cell lines from *Ern1*^{S724A/S724A} mice and their *Ern1*^{WT/WT} littermates to evaluate the effect of phosphorylation at Ser⁷²⁴ upon the kinase activity of IRE1 α for autophosphorylation at other sites and consequently upon the activation of its RNase activity as well. Utilizing Phos-tag gel-based immunoblot analyses (39, 40), we measured the overall phosphorylation states of IRE1 α protein in MEF cells in response to chemical ER stress. In *Ern1*^{WT/WT} control MEF cells treated with 10 μ g/ml Tm or 1 μ M Tg, we observed apparently slow-migrating IRE1 α protein from the Phos-tag gel because of its robust autophosphorylation (Fig. 2A), which was in parallel with phosphorylation at Ser⁷²⁴ as detected by the phospho-IRE1 α antibody and could be efficiently blocked by KIRA6, an IRE1 α kinase inhibitor (41) (Fig. 2A). By contrast, abrogation of Ser⁷²⁴ phosphorylation markedly reduced autophosphorylation, conceivably at other sites, of IRE1 α -S724A protein in *Ern1*^{S724A/S724A} MEF cells upon ER stress (Fig. 2A). Corresponding to its lower autophosphorylation states, S724A mutation of IRE1 α resulted in significant decreases in *Xbp1* mRNA splicing and mRNA abundance of *Erdj4*, an XBP1s target gene, along with significantly increased mRNA abundance of *Blos1*, a typical RIDD target that affects the cellular behavior and function of

Phosphorylation regulation of IRE1 α activation

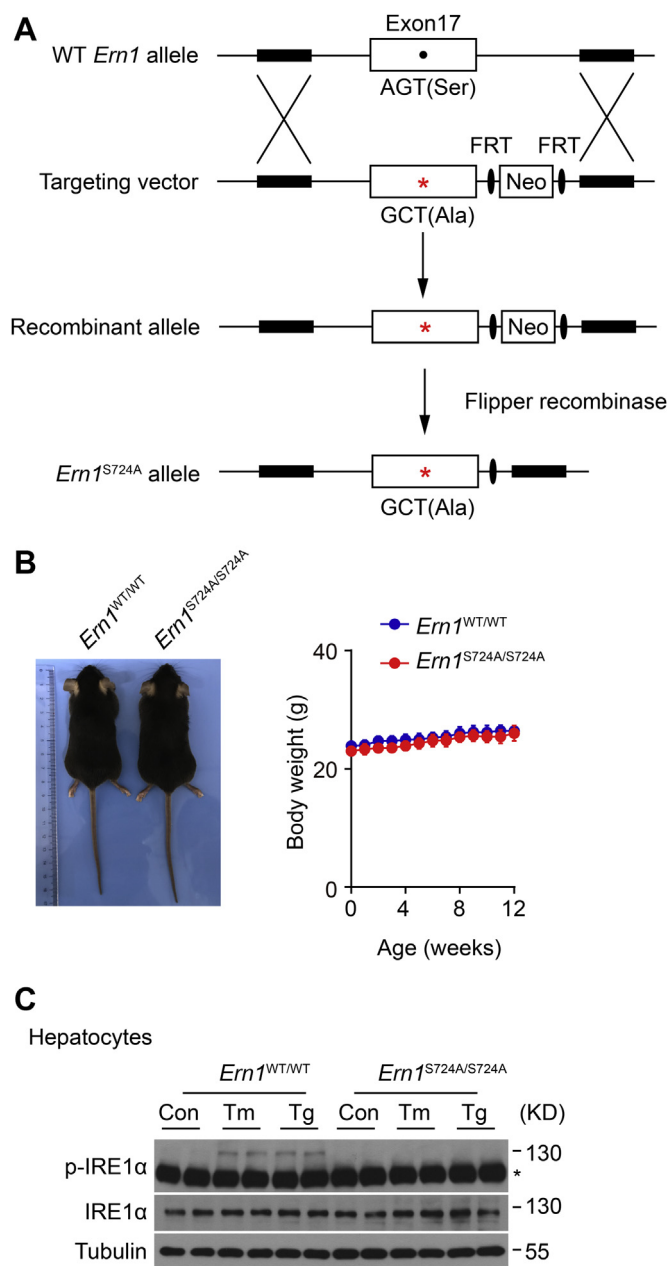


Figure 1. Creation of *Ern1*^{S724A} knock-in mutant mouse model. A, schematic illustration of the gene targeting strategy for creating *Ern1*^{S724A} knock-in mutant line. The targeting vector contains exon 17 in which the Ser (S, AGT) residue at 724 was substituted with Ala (A, GCT) in the mouse *Ern1* gene, and the FRT-flanked Neomycin (Neo) cassette was subsequently removed by Flipper recombinase. B, photograph of *Ern1*^{S724A/S724A} mice and *Ern1*^{WT/WT} littermates and their body weight when maintained on a normal chow diet at the indicated ages (n = 4 per group). C, immunoblot analysis of IRE1 α phosphorylation at Ser⁷²⁴ in primary hepatocytes from *Ern1*^{WT/WT} control and *Ern1*^{S724A/S724A} mice. Hepatocytes were treated with the chemical ER stressors tunicamycin (Tm, 10 μ g/ml) for 4 h or thapsigargin (Tg, 1 μ M) for 2 h. The asterisk indicates a nonspecific band detected by anti-phospho-IRE1 α antibody. Tubulin was used as the loading control. ER, endoplasmic reticulum; IRE1 α , inositol-requiring enzyme 1 α .

lysosomes (42), in *Ern1*^{S724A/S724A} MEF cells relative to WT *Ern1*^{WT/WT} control cells (Fig. 2, B and C). To further affirm the effect of S724A mutation upon the RNase activation of IRE1 α , we overexpressed by adenovirus infection IRE1 α -S724A protein in primary hepatocytes isolated from liver-specific IRE1 α knockout (LKO) mice (43) (Fig. 2D). Whereas overexpression

of the WT IRE1 α protein led to robust *Xbp1* mRNA splicing and detectable XBP1s production that could be further increased upon treatment with 1 μ M Tg, S724A mutation significantly reduced them under both conditions (Fig. 2E). However, IRE1 α -S724A protein possessed significant *Xbp1* mRNA splicing activity in comparison to its kinase-dead IRE1 α -K599A or RNase-dead K907A mutant protein (44) (Fig. 2E). These results indicate that loss of Ser⁷²⁴ phosphorylation reduces the kinase activity of IRE1 α for autophosphorylation at other sites, leading to blunted RNase activity and *Xbp1* mRNA splicing during ER stress.

Phosphorylation at Ser⁷²⁴ affects the dynamic activation of IRE1 α

To test whether inactivation of Ser⁷²⁴ phosphorylation influences the dynamic features of IRE1 α autophosphorylation in association with its functional outputs of RNase activity, we first measured the dose-responsive activation of IRE1 α RNase activity in MEF cells treated for 24 h with Tm at a range of 0.05 to 0.25 μ g/ml. Quantitative RT-PCR analysis revealed rapid elevations in *Xbp1* mRNA splicing and *Erdj4* mRNA levels, as well as a swift decrease in *Blos1* mRNA abundance, upon treatment with 0.05 μ g/ml Tm, reaching a maximum at 0.15 μ g/ml Tm for *Xbp1* mRNA splicing and at 0.1 μ g/ml Tm for RIDD of *Blos1* mRNA in *Ern1*^{WT/WT} control MEF cells (Fig. 3A). By contrast, regardless of the Tm doses tested, abrogation of Ser⁷²⁴ phosphorylation resulted in a steady ~40% reduction in the activity of IRE1 α for *Xbp1* mRNA splicing, and a complete loss of its activity for RIDD of *Blos1* mRNA, in *Ern1*^{S724A/S724A} MEF cells (Fig. 3A). Next, we examined by Phos-tag gel analysis, the phosphorylation states of IRE1 α at different time intervals during relatively mild ER stress induced by 0.1 μ g/ml Tm, and we detected a majority of robustly phosphorylated IRE1 α protein that increased in a time-dependent fashion after Tm treatment in *Ern1*^{WT/WT} cells (Fig. 3B). Interestingly, we also observed some very minor super-shifted species, likely representing IRE1 α protein molecules that possessed more residues undergoing autophosphorylation. In comparison, S724A mutation resulted in dramatic decreases in the amount of autophosphorylated IRE1 α -S724A protein in *Ern1*^{S724A/S724A} cells even after 24 h of Tm treatment, which also exhibited an appreciably lower shift relative to its WT counterpart in *Ern1*^{WT/WT} cells (Fig. 3B). In parallel with the phosphorylation levels of IRE1 α protein, production of XBP1s protein (Fig. 3B) as well as its mRNA splicing (Fig. 3, C and D) reached to their highest levels at 12 and 16 h, respectively, after Tm treatment in *Ern1*^{WT/WT} MEF cells; whereas significant reductions in XBP1s protein production (Fig. 3B) and its mRNA splicing (Fig. 3, C and D) were observed in *Ern1*^{S724A/S724A} cells. Consistently, no decrease in *Blos1* mRNA abundance was detected in *Ern1*^{S724A/S724A} MEF cells (Fig. 3D). Then, we treated MEF cells with higher concentration of Tm at 10 μ g/ml and asked if S724A mutation could impact the kinase/RNase activity of IRE1 α under a more severe ER stress condition. Phos-tag gel analysis showed marked phosphorylation of IRE1 α protein at

Phosphorylation regulation of IRE1 α activation

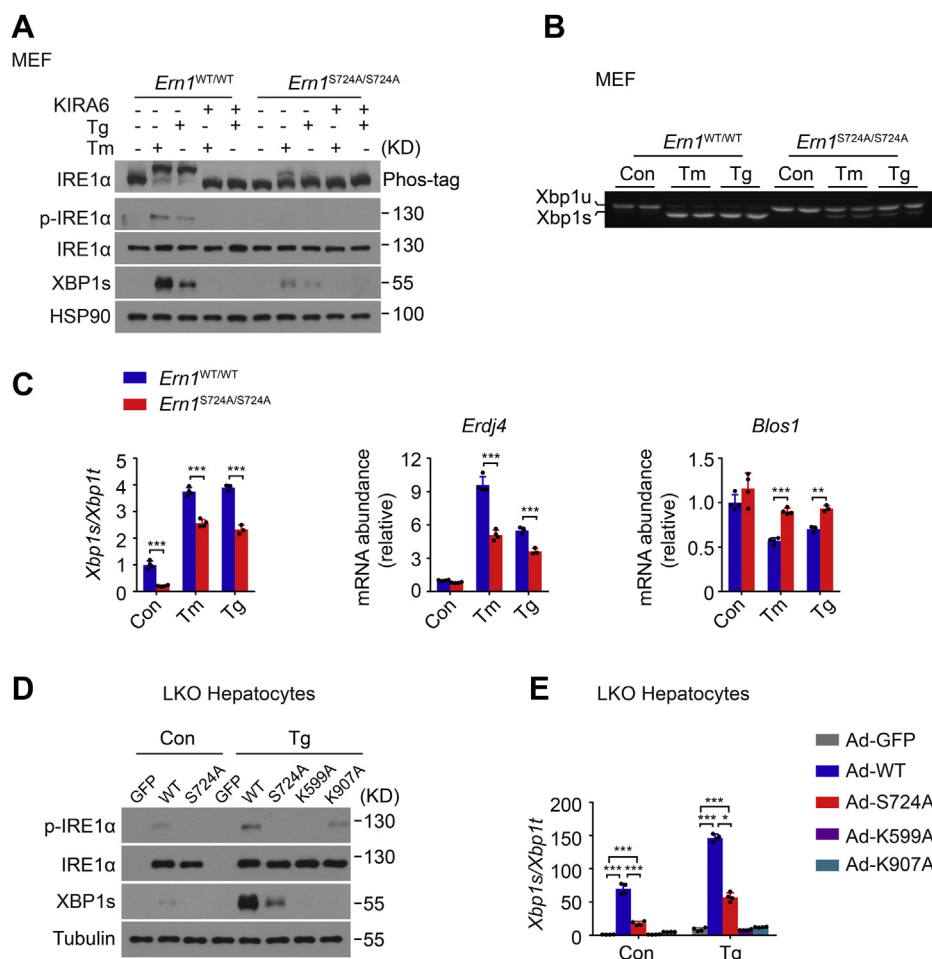


Figure 2. S724A mutation results in lower IRE1 α autophosphorylation with reduced RNase activity upon ER stress. *A*, MEF cells derived from *Em1*^{WT/WT} and *Em1*^{S724A/S724A} mice were treated with DMSO (–), 10 μ M Tm, for 4 h or 1 μ M Tg for 2 h after preincubation for 30 min with DMSO (–) or 10 μ M KIRA6, the IRE1 α kinase inhibitor. Immunoblot analysis of IRE1 α autophosphorylation by Phos-tag gel and its phosphorylation at Ser⁷²⁴ using anti-phospho-IRE1 α antibody. HSP90 was used as the loading control. *B* and *C*, MEF cells of the indicated genotypes were likewise treated with DMSO (Con), Tm, or Tg. *B*, agarose gel analysis of *Xbp1* mRNA splicing by RT-PCR. Shown are PCR products corresponding to the unspliced *Xbp1u* and spliced *Xbp1s* mRNA. *C*, quantitative RT-PCR analysis of *Xbp1* mRNA splicing, shown as the ratio of spliced (*Xbp1s*) to total (*Xbp1t*) *Xbp1* mRNA, along with the abundance of *Erdj4* and *Blos1* mRNA. *D* and *E*, primary hepatocytes from male liver-specific IRE1 α knockout (LKO) mice were infected for 48 h with adenoviruses expressing GFP, WT, or the indicated mutant human IRE1 α proteins and subsequently treated for 2 h with DMSO (Con) or 1 μ M Tg. *D*, immunoblot analysis of IRE1 α protein and its phosphorylation at Ser⁷²⁴, along with the production of XBP1s protein. Tubulin was used as the loading control. *E*, quantitative RT-PCR analysis of *Xbp1* mRNA splicing. All data are presented as the mean \pm SD ($n = 2$ or 3 independent experiments). * $p < 0.05$, ** $p < 0.01$, *** $p < 0.001$ by two-tailed unpaired Student's *t* test. DMSO, dimethyl sulfoxide; ER, endoplasmic reticulum; HSP90, heat shock protein 90; IRE1 α , inositol-requiring enzyme 1 α ; MEF, mouse embryonic fibroblast; RNase, ribonuclease; Tg, thapsigargin; *Xbp1*, X-box binding protein 1.

6 h following high Tm treatment, which was sustained at similar levels thereafter in *Em1*^{WT/WT} cells (Fig. 3E). This was accompanied by highly robust *Xbp1* mRNA splicing maintained at similar levels throughout the period of high Tm treatment from 6 to 24 h (Fig. 3, F and G), along with rapid and gradual decreases in *Blos1* mRNA abundance (Fig. 3G). In *Em1*^{S724A/S724A} MEF cells, by contrast, stimulation with high Tm resulted in similarly rapid occurrence of phosphorylated IRE1 α -S724A protein that was obviously less abundant and shifted lower in comparison to their WT counterparts and did not increase in a time-dependent manner (Fig. 3E). In correspondence to the altered phosphorylation states of IRE1 α -S724A protein, ~40 to 60% reductions were observed in its activities for *Xbp1* mRNA splicing and *Blos1* mRNA degradation (Fig. 3, F and G). Unlike that under mild ER stress state, IRE1 α -S724A protein exhibited a considerable RIDD activity

for *Blos1* mRNA upon severe ER stress induced by high Tm (Fig. 3G). Interestingly, we observed a high amount of XBP1s protein induced at 6 h that decreased in *Em1*^{WT/WT} cells at 24 h following high Tm treatment, while detecting an apparently lower amount of XBP1s protein that similarly decreased in *Em1*^{S724A/S724A} cells after 24 h of high Tm treatment (Fig. 3E). This may indicate similar turnover rate of XBP1s protein in these two types of MEF cells during severe ER stress.

Given the critical role of the IRE1 α branch in cell fate control (4), we wondered if this dynamic impairment of IRE1 α RNase activation is coupled to cell survival during ER stress. Curiously, at 6 h but not at 24 h following treatment with high Tm at 10 μ M, we observed decreased PERK phosphorylation along with lower protein level of the transcription factor CCAAT-enhancer binding protein homologous protein (CHOP) in *Em1*^{S724A/S724A} MEF cells (Fig. 4A), which was in

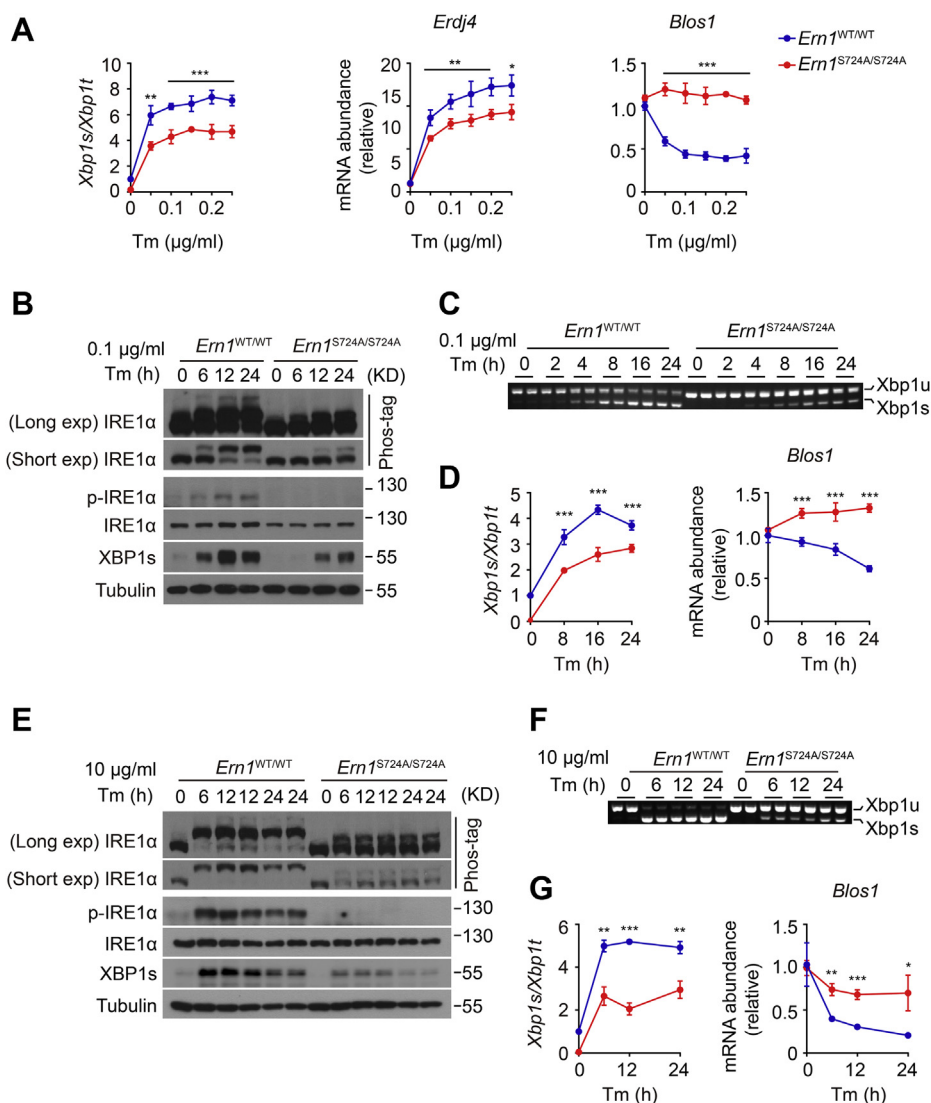


Figure 3. Effects of S724A mutation upon the dynamic activation of IRE1 α in MEF cells. *A*, MEF cells of the indicated genotypes were treated with Tm at the indicated concentrations for 24 h. Quantitative RT-PCR analysis of *Xbp1* mRNA splicing and the mRNA abundance of the indicated genes. *B–G*, MEF cells were treated with 100 ng/ml or 10 μ g/ml Tm for the indicated time intervals. *B* and *E*, immunoblot analysis of IRE1 α phosphorylation and XBP1s protein. Upper Phos-tag gels with long or short exposure time are shown for the band-shift analysis of IRE1 α protein phosphorylation. Tubulin was used as the loading control. *C* and *F*, agarose gel analysis of *Xbp1* mRNA splicing by RT-PCR. *D* and *G*, quantitative RT-PCR analysis of *Xbp1* mRNA splicing and the RIDD target *Bloss1* mRNA. All data are presented as the mean \pm SD ($n = 3$ independent experiments). * $p < 0.05$, ** $p < 0.01$, *** $p < 0.001$ by two-tailed unpaired Student's t test or two-way ANOVA. IRE1 α , inositol-requiring enzyme 1 α ; MEF, mouse embryonic fibroblast; RIDD, regulated IRE1-dependent decay; Tm, tunicamycin; *Xbp1*, X-box binding protein 1; XBP1s, spliced XBP1.

accordance with lower accumulation of CHOP protein detected in the nucleus at this particular stage of ER stress (Fig. 4*B*). Consistently, a significant, though not dramatic, improvement in cell viability, as well as a lower level of the cleaved form of caspase-3, was observed in stressed $Em1^{S724A/S724A}$ MEF cells at 6 h after Tm treatment (Fig. 4, *C* and *D*). This indicates that loss of Ser⁷²⁴ phosphorylation of IRE1 α may promote MEF cell survival even in the face of impaired production of XBP1s at early stages of ER stress, likely through attenuating the PERK-CHOP pathway.

Next, we considered if inactivation of Ser⁷²⁴ phosphorylation could impact the dynamic activation of IRE1 α in a cell type-dependent fashion. Using isolated primary hepatocytes from $Em1^{WT/WT}$ and $Em1^{S724A/S724A}$ mice, Phos-tag gel analyses revealed obvious decreases in Tm- or Tg-induced

autophosphorylation of IRE1 α -S724A protein with less shifting relative to its WT counterpart (Fig. 5*A*), which is analogous to our observations in MEF cells (Fig. 2*A*). Under mild ER stress induced by 0.1 μ g/ml Tm, we observed overt reductions in autophosphorylation of IRE1 α -S724A protein in $Em1^{S724A/S724A}$ hepatocytes relative to its WT counterpart in $Em1^{WT/WT}$ hepatocytes (Fig. 5*B*). Interestingly, Tm treatment induced a time-dependent increase in IRE1 α protein level in both hepatocytes (Fig. 5*B*), which was not observed in MEF cells; and Tm-induced phosphorylation of IRE1 α -S724A protein appeared to be higher in $Em1^{S724A/S724A}$ hepatocytes than that in $Em1^{S724A/S724A}$ MEF cells, particularly at 24 h after Tm treatment (Figs. 3*B* and 5*B*). Whereas *Xbp1* mRNA splicing was maintained at similar levels in $Em1^{WT/WT}$ control hepatocytes after 8 h of Tm treatment, it was decreased to a

Phosphorylation regulation of IRE1 α activation

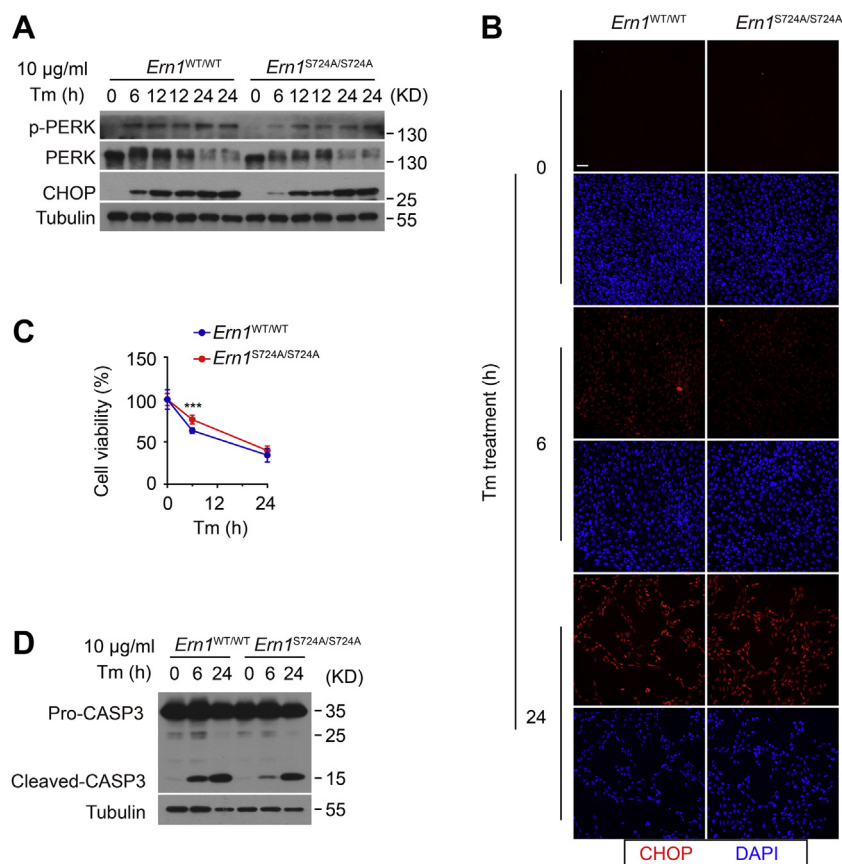


Figure 4. Effects of S724A mutation upon cell survival under ER stress in MEF cells. MEF cells of the indicated genotypes were treated with 10 μ g/ml Tm for the indicated time intervals. *A*, immunoblot analysis of PERK phosphorylation and CHOP protein levels. Tubulin was used as the loading control. *B*, immunofluorescence staining of CHOP protein along with DAPI staining in MEF cells following Tm treatment. The scale bar represents 50 μ m. *C*, cell viability of Tm-treated MEF cells was determined by CCK8 assay. Shown is the percentage of viability after normalization to their untreated controls. *D*, immunoblot analysis of cleavage of caspase-3 protein. Tubulin was used as the loading control. Data are presented as the mean \pm SD ($n = 3$ independent experiments). *** $p < 0.001$ by two-tailed unpaired Student's t test. CCK8, Cell Counting Kit-8; CHOP, CCAAT-enhancer binding protein homologous protein; DAPI, 4',6-diamidino-2-phenylindole; ER, endoplasmic reticulum; MEF, mouse embryonic fibroblast; PERK, PKR-like endoplasmic reticulum kinase; Tm, tunicamycin.

similar extent (by $\sim 25\%$) in *Ern1*^{S724A/S724A} hepatocytes (Fig. 5C). Unlike our observations in MEF cells (Fig. 3D), S724A mutation resulted in significant reductions in, but not a complete loss of, its RIDD activity for *Blos1* mRNA (Fig. 5C). Under severe ER stress induced by 10 μ g/ml Tm, we observed similar effects of S724A mutation upon IRE1 α autophosphorylation states and XBP1s protein production (Fig. 5D) in association with its RNase activities (Fig. 5E) in *Ern1*^{S724A/S724A} hepatocytes. Notably, at 24 h after Tm treatment, CHOP protein levels appeared to be elevated in *Ern1*^{S724A/S724A} hepatocytes (Fig. 5, B and D). However, relative to *Ern1*^{WT/WT} hepatocytes, no changes in cell viability were detected in *Ern1*^{S724A/S724A} hepatocytes (Fig. 5F), despite that appreciably higher nuclear accumulation of CHOP protein was found in *Ern1*^{S724A/S724A} hepatocytes at 24 h following high Tm treatment (Fig. 5G). This may reflect a unique ability of hepatocytes to counteract ER stress-associated cell death without involving the CHOP pathway, which has been frequently shown to mediate apoptosis in other cell types (4).

Taken together, these results from MEF cells and hepatocytes demonstrate an important role of phosphorylation at Ser⁷²⁴ in governing the kinase activity of IRE1 α for its further autophosphorylation, which is closely coupled to the activation

mode of its RNase activity. Abrogation of phosphorylation at this particular site of the kinase activation loop is likely to cause intrinsic defect in the ability of IRE1 α to autophosphorylate sufficiently at additional sites, which are supposed to be needed for its activation to the fullest capacity. Unlike the documented phosphorylation at Ser⁷²⁹ that preferably responds to TLR agonists and primarily regulates its RIDD activity (38), phosphorylation at Ser⁷²⁴ of IRE1 α may represent a universal event during its activation upon ER stress, which controls its functional RNase output for both *Xbp1* mRNA splicing and RIDD of select RNA substrates. It is currently unclear whether the cell type-selective feature of IRE1 α -S724A mutant's RIDD activity reflects its distinct phosphorylation states exerting an impact upon possible auxiliary factors in the RIDD machinery in different types of cells. In addition, phosphorylation at Ser⁷²⁴ of IRE1 α may also exert differing cell type-dependent effects upon cell survival under ER stress.

Abrogation of IRE1 α phosphorylation at Ser⁷²⁴ exacerbates ER stress-induced hepatic steatosis

ER stress is a key feature in hepatic steatosis and nonalcoholic fatty liver disease (45–47), and the IRE1 α -XBP1 pathway

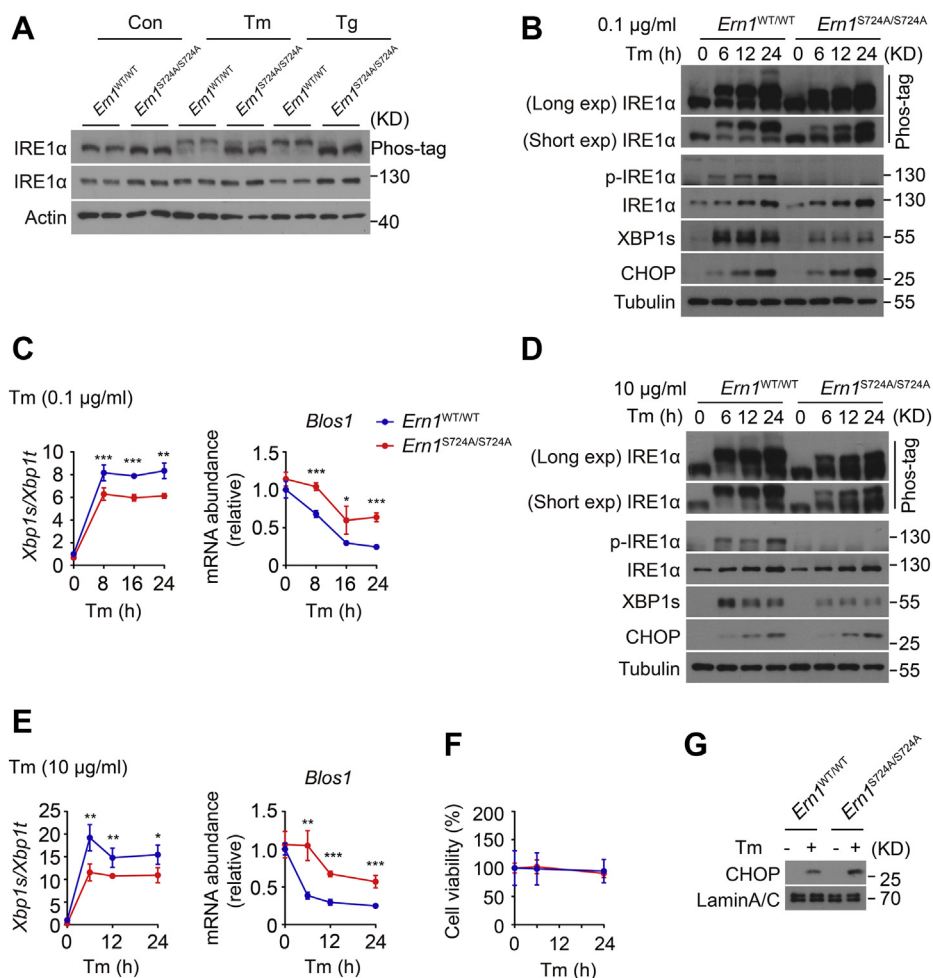


Figure 5. Disruption of Ser⁷²⁴ phosphorylation attenuates the RNase activation of IRE1 α in hepatocytes. *A*, primary hepatocytes from mice of the indicated genotypes were treated with DMSO control (Con), 10 μ g/ml Tm for 4 h, or 1 μ M Tg for 2 h. Immunoblot analysis of IRE1 α protein, with upper Phos-tag gel analysis of IRE1 α phosphorylation. Actin was used as the loading control. *B–E*, hepatocytes of the indicated genotypes were treated with 100 ng/ml or 10 μ g/ml Tm for the indicated time intervals. *B* and *D*, immunoblot analysis of IRE1 α phosphorylation along with XBP1s and CHOP protein levels. Upper Phos-tag gels are shown for the band-shift analysis of IRE1 α protein phosphorylation with long or short exposure time. Tubulin was used as the loading control. *C* and *E*, quantitative RT–PCR analysis of *Xbp1* mRNA splicing and the RIDD target *Bloss1* mRNA. *F* and *G*, hepatocytes were treated with 10 μ g/ml Tm. *F*, cell viability analysis by CCK8 assay. *G*, immunoblot analysis of nuclear CHOP protein after 24 h of 10 μ g/ml Tm treatment. Lamin A/C was used as the nuclear protein control. All data are presented as the mean \pm SD ($n = 2$ or 3 independent experiments). * $p < 0.05$, ** $p < 0.01$, and *** $p < 0.001$ by two-tailed unpaired Student's *t* test or two-way ANOVA. CCK8, Cell Counting Kit-8; CHOP, CCAAT-enhancer binding protein homologous protein; DMSO, dimethyl sulfoxide; IRE1 α , inositol-requiring enzyme 1 α ; RIDD, regulated IRE1-dependent decay; RNase, ribonuclease; Tg, thapsigargin; Tm, tunicamycin; XBP1s, spliced X-box binding protein 1.

has been implicated in the control of many aspects of hepatic lipid homeostasis, including *de novo* lipogenesis, fatty acid β -oxidation, and lipid secretion (43, 48–50). Given that IRE1 α was documented to have a protective role in ER stress-induced liver steatosis (51, 52), we sought to determine the physiological importance of phosphorylation at Ser⁷²⁴ of IRE1 α during its activation in the liver in response to chemical ER stress in Tm-treated mice. Abrogation of Ser⁷²⁴ phosphorylation of IRE1 α resulted in more severe hepatic steatosis, that is, higher accumulation of liver lipids as determined by Oil-Red O staining, in *Em1^{S724A/S724A}* mice than their *Em1^{WT/WT}* control group following 6 or 24 h of Tm treatment (Fig. 6, *A* and *B*). Consistently, imaging analysis by hyperspectral stimulated Raman scattering (hsSRS) of liver sections (53) also revealed significant elevations in hepatic lipid content (Fig. 5*C*), but no alterations in the unsaturated ratio of lipids

(Fig. 6*D*) in Tm-treated *Em1^{S724A/S724A}* mice relative to *Em1^{WT/WT}* mice were revealed. Furthermore, more progressive increases in triacylglycerides (TG) levels were detected in the livers of *Em1^{S724A/S724A}* mice than their *Em1^{WT/WT}* counterparts following 6 and 24 h of Tm treatment, which was accompanied by higher decreases in their serum TG levels (Fig. 6*E*). These results indicate that inactivation of Ser⁷²⁴ phosphorylation of IRE1 α functionally impairs its ability to regulate hepatic lipid metabolism, leading to higher liver accumulation with lower secretion of neutral lipids, that is, exacerbation of ER stress-induced liver steatosis.

Because hepatic lipid accumulation dynamically involves metabolic pathways including *de novo* lipogenesis, fatty acid oxidation, as well as lipid secretion and uptake, we next examined whether impairment of IRE1 α phosphorylation affected the related gene expression programs in the livers of

Phosphorylation regulation of IRE1 α activation

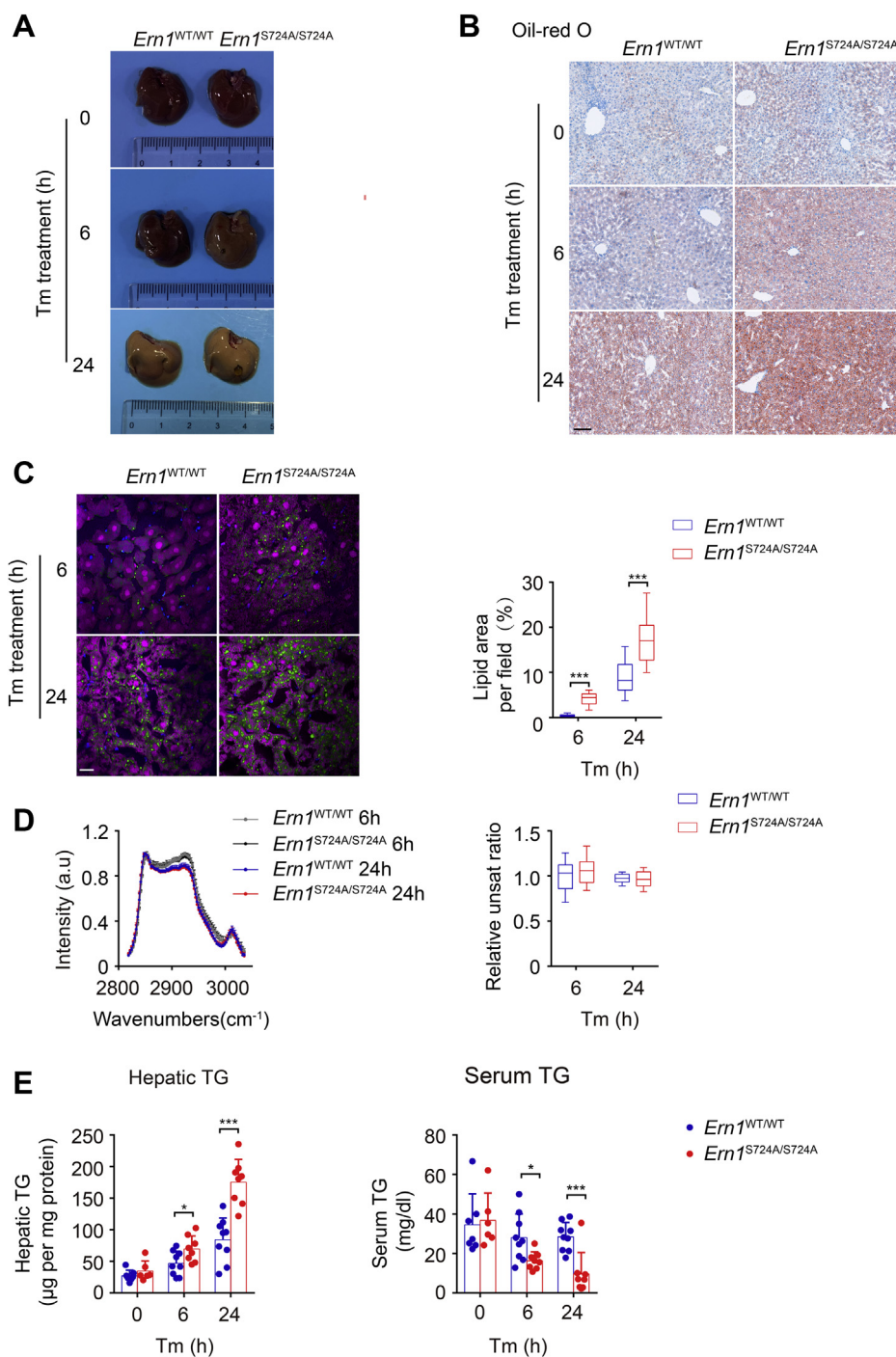


Figure 6. S724A mutation of IRE1 α results in aggravated hepatic steatosis with reduced plasma lipids under ER stress. Male *Em1*^{S724A/S724A} mice and their *Em1*^{WT/WT} littermates at 2 months of age were injected i.p. with Tm (1 mg/kg body weight) and sacrificed at 6 or 24 h after Tm treatment ($n = 6-9$ per group). Mice treated with 150 μ M dextrose was used as the vehicle control group. **A**, representative liver images. **B**, representative images of Oil-Red O staining of livers ($n = 3$ per group). The scale bar represents 100 μ m. **C**, representative hsSRS images of liver sections from mice at 6 and 24 h after Tm injection. Imaging analysis by the Multivariate Curve Resolution (MCR) algorithm showing chemical distributions of lipid (green), lipofuscin (blue), and protein (magenta) in a field of $200 \times 200 \mu\text{m}^2$ (300×300 pixels with dwell time of 10 μ s/pixel for imaging). Lipid contents were quantified as areas of lipid signals per field using ImageJ ($n = 3$ per group). The scale bar represents 20 μ m. **D**, the average hsSRS spectra of hepatic lipids. The Raman peak at 3007 cm^{-1} represents the vibration from unsaturated =CH stretch. The degree of lipid unsaturation was evaluated by the ratio of Raman intensity at 3007 and 2853 cm^{-1} . **E**, liver and serum levels of triglycerides. Data represent the mean \pm SD. * $p < 0.05$, *** $p < 0.001$ by two-tailed unpaired Student's t test. ER, endoplasmic reticulum; hsSRS, hyperspectral stimulated Raman scattering; IRE1 α , inositol-requiring enzyme 1 α ; Tm, tunicamycin.

Em1^{S724A/S724A} mice. Quantitative RT-PCR profiling revealed significantly blunted induction of *Xbp1* mRNA splicing and *Erdj4* mRNA expression in *Em1*^{S724A/S724A} livers at 6 and 24 h after Tm treatment (Fig. 7A), suggesting a lower RNase activity

of the IRE1 α -S724A protein *in vivo*. Surprisingly, while no significant changes were detected in Tm stimulation of binding immunoglobulin protein (*Bip*) mRNA expression, significantly higher upregulation of *Chop* mRNA was observed in

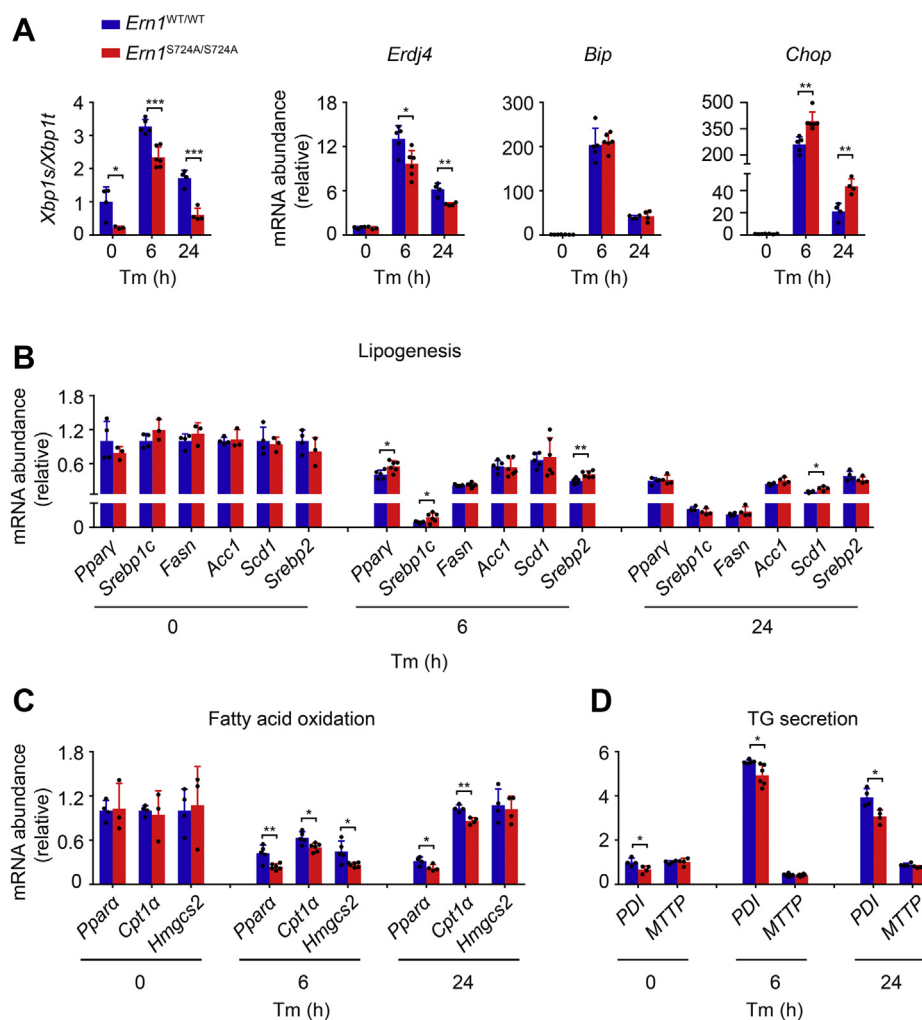


Figure 7. Effects of S724A mutation of IRE1 α upon hepatic gene expression programs related to ER stress and lipid metabolism. Quantitative RT-PCR analysis of the mRNA abundance of the indicated genes in livers of *Em1*^{S724A/S724A} mice and their *Em1*^{WT/WT} littermates following treatment with Tm or vehicle (n = 3–6 per group). *A*, the UPR genes. *B*, lipogenesis. *C*, fatty acid β -oxidation. *D*, TG secretion. Data are presented as the mean \pm SD. **p* < 0.05, ***p* < 0.01, and ****p* < 0.001 by two-tailed unpaired Student's *t* test. ER, endoplasmic reticulum; IRE1 α , inositol-requiring enzyme 1 α ; TG, triacylglyceride; Tm, tunicamycin; UPR, unfolded protein response.

Em1^{S724A/S724A} livers (Fig. 7A). In parallel, whereas Tm treatment exerted a suppressive effect upon the expression of key transcriptional regulators and metabolic enzymes in both lipogenesis and fatty acid oxidation (Fig. 7, B and C), we detected significant increases in the expression of lipogenic genes, including peroxisome proliferator-activated receptor gamma (*Ppar* γ), sterol regulatory element-binding transcription factor 1 (*Srebp1c*), and *Scd1* (Fig. 7B), along with significant decreases in that of genes related to fatty acid oxidation such as *Ppara* and *Cpt1 α* (Fig. 7C), in *Em1*^{S724A/S724A} livers at 6 or 24 h after Tm treatment. These data suggest that the lowered RNase activity of IRE1 α -S724A protein resulted in decreased *Xbp1* mRNA splicing, along with enhanced expression of *Chop*, which also has been shown to be a key mediator in ER stress-induced suppression of genes related to lipid metabolism in hepatic steatosis (54). Moreover, in the livers of *Em1*^{WT/WT} control mice, we observed marked Tm-induced upregulation of *PDI* (encoding protein disulfide isomerase [PDI]) but not *MTTP* (encoding microsomal

triglyceride-transfer protein [MTTP]) (Fig. 7D), and a significant attenuation of Tm-induced upregulation of *PDI* was seen in *Em1*^{S724A/S724A} livers (Fig. 7D). This blunted expression of *PDI*, a crucial regulator of TG secretion from the liver, could also be ascribable to the weakened activation of *Xbp1* mRNA splicing in *Em1*^{S724A/S724A} livers, which is in line with the reported findings (50).

IRE1 α regulates hepatic expression of CHOP and PDI through XBP1s under ER stress

Next, we asked if the dampened production of XBP1s could mechanistically link the insufficient activation of IRE1 α to the altered expression of CHOP and PDI in the liver. Consistently, immunoblot analysis showed that abrogation of Ser⁷²⁴ phosphorylation of IRE1 α resulted in marked reductions in hepatic XBP1s protein production in *Em1*^{S724A/S724A} mice at 6 or 24 h after Tm treatment (Fig. 8, A–D). Interestingly, decreased Tm-induced phosphorylation of PERK but unaltered BiP

Phosphorylation regulation of IRE1 α activation

protein expression was detected, indicating a likely connection between Ser⁷²⁴ phosphorylation of IRE1 α and PERK activation. However, robust elevations in CHOP protein levels were seen in *Ern1*^{S724A/S724A} livers (Fig. 8, A–D), somewhat similar to our observations in primary hepatocytes (Fig. 5, B and D). Thus, such increased CHOP expression was unrelated to the PERK pathway in ER-stressed *Ern1*^{S724A/S724A} livers. Moreover, we

observed significantly reduced PDI protein level along with higher abundance of adipose differentiation–related protein (ADRP), the cytosolic lipid droplet protein marker, but detected no prominent changes in the lipogenic enzymes, fatty acid synthase and acetyl-CoA carboxylase 1 (ACC1), or in the key lipogenic transcription factor SREBP1c, in *Ern1*^{S724A/S724A} livers relative to their *Ern1*^{WT/WT} counterparts following Tm

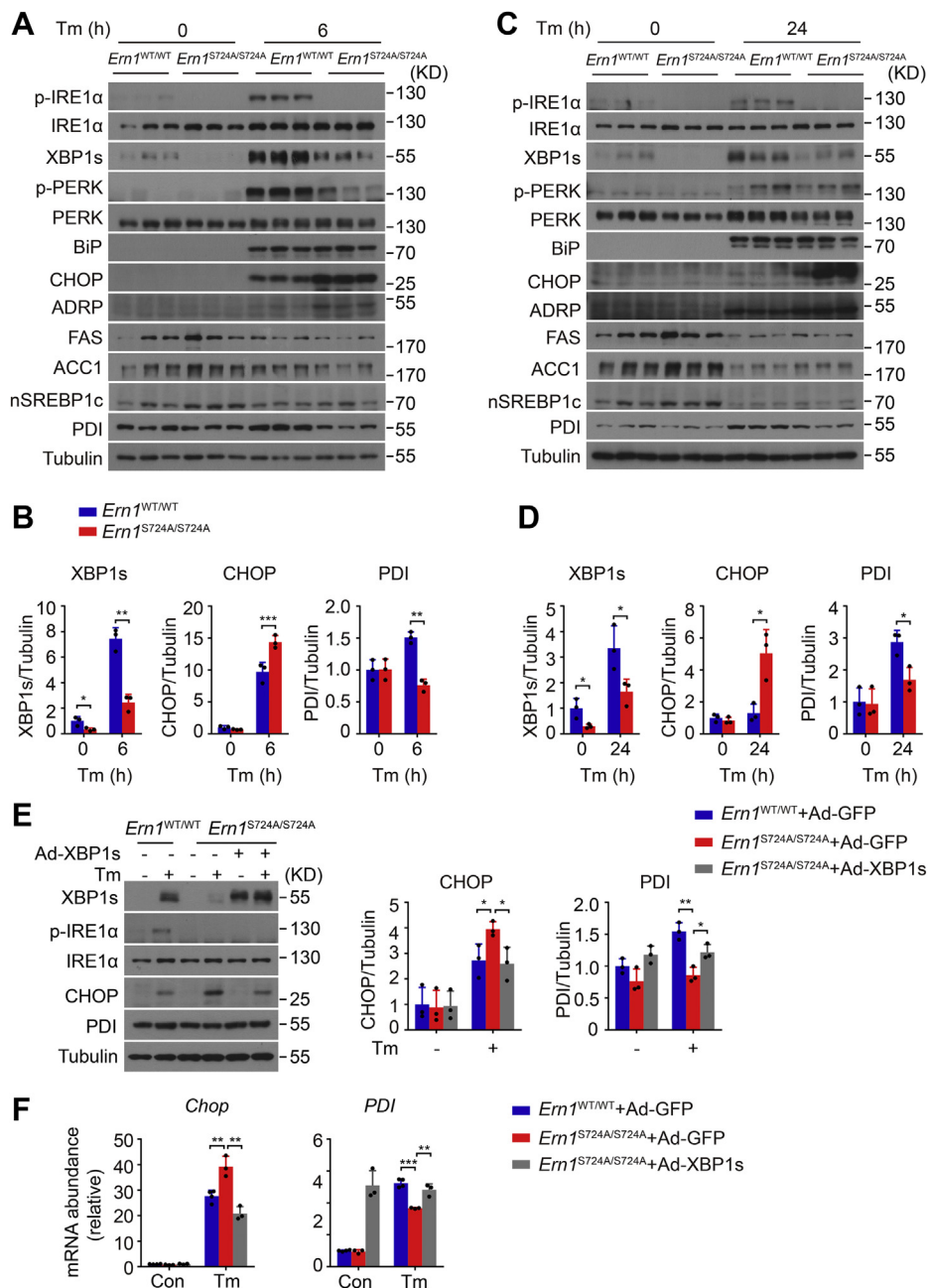


Figure 8. S724A mutation of IRE1 α results in blunted XBP1s production with decreased PDI but increased CHOP expression in ER-stressed livers. A–D, immunoblot analysis of the phosphorylation and expression levels of the indicated proteins in livers of *Ern1*^{S724A/S724A} mice and their *Ern1*^{WT/WT} littermates following treatment with Tm or vehicle for 6 h (A and B) or 24 h (C and D). Shown are representative immunoblots for three individual mice per group (A and C), and quantification of XBP1s, PDI, and CHOP protein levels after normalization to tubulin (B and D). E and F, primary hepatocytes from male *Ern1*^{S724A/S724A} mice and their *Ern1*^{WT/WT} littermates were infected for 30 h with adenoviruses expressing GFP control or XBP1s protein. Cells were then treated with Tm (100 ng/ml) for 24 h. E, immunoblot analysis of XBP1s protein, IRE1 α phosphorylation, as well as PDI and CHOP proteins. Shown also is the quantification of PDI and CHOP protein levels after normalization to tubulin as the loading control. F, quantitative RT–PCR analysis of the mRNA abundance of the indicated genes. Results in (E) and (F) represent three independent experiments. All data are presented as the mean \pm SD. * p < 0.05, ** p < 0.01, and *** p < 0.001 by two-tailed unpaired Student's t test or two-way ANOVA. CHOP, CCAAT-enhancer binding protein homologous protein; ER, endoplasmic reticulum; IRE1 α , inositol-requiring enzyme 1 α ; PDI, protein disulfide isomerase; Tm, tunicamycin; XBP1s, spliced X-box binding protein 1.

treatment (Fig. 8, A–D). These data indicate that in accordance with their mRNA expression levels, deficient production of XBP1s protein was indeed coupled with persistently higher CHOP protein and lower PDI protein expression levels without apparently increasing the ER stress state in the livers of Tm-treated *Ern1*^{S724A/S724A} mice.

To test whether XBP1s mediates the effects of IRE1 α –S724A upon the expression levels of CHOP and PDI, we used adenovirus to overexpress XBP1s protein in primary hepatocytes isolated from *Ern1*^{S724A/S724A} mice. Similar to our observations in the liver, significant increases in Tm induction of CHOP protein as well as its mRNA expression were detected, and restored expression of XBP1s significantly blunted both in *Ern1*^{S724A/S724A} hepatocytes (Fig. 8, E and F). In addition, S724A mutation of IRE1 α also suppressed Tm-induced elevations in PDI protein as well as its mRNA expression levels, and overexpression of XBP1s reversed both in *Ern1*^{S724A/S724A} hepatocytes (Fig. 8, E and F). Thus, deficient production of XBP1s, at least in large part, mediated the persistent upregulation of CHOP as well as the downregulation of PDI in hepatocytes, thereby promoting the aggravation of ER stress-induced hepatic steatosis.

Finally, we went on to examine whether increased hepatic CHOP protein levels were associated with cell death in livers of Tm-treated *Ern1*^{S724A/S724A} mice. Consistently, immunostaining of liver sections revealed apparently higher intensity of CHOP protein signals (Fig. 9A), and immunoblot analysis

showed increased nuclear accumulation of CHOP protein (Fig. 9B), in livers of *Ern1*^{S724A/S724A} mice after 6 or 24 h of Tm treatment. However, we neither observed detectable levels of the cleaved form of caspase-3 (Fig. 9C) nor found appreciable apoptosis signals by TUNEL analysis, in *Ern1*^{S724A/S724A} or *Ern1*^{WT/WT} livers at 24 h following Tm treatment (Fig. 9D). These results further support the notion that CHOP protein may mainly contribute to the dysregulation of hepatic lipid metabolism, rather than mediating cellular apoptosis, during ER stress-induced hepatosteatosis (54).

Discussion

Autophosphorylation of IRE1 α has been established as a key step in its functional activation, but it has yet to be fully understood how its phosphorylation states are endogenously regulated and coupled to its RNase outputs in response to various stress states. In the current study, we investigated the role *in vivo* of phosphorylation at Ser⁷²⁴, one of the three serine residues (Ser⁷²⁴, Ser⁷²⁶, and Ser⁷²⁹) within the kinase activation loop of IRE1 α that are known to undergo phosphorylation during its activation upon ER stress (36, 37). Our results revealed that phosphorylation at Ser⁷²⁴ critically governs IRE1 α kinase activity for its autophosphorylation at other sites, which presumably enables the full activation of its RNase activity for both *Xbp1* mRNA splicing and RIDD of *Blos1* mRNA substrate. Furthermore, using *Ern1*^{S724A/S724A} knock-in

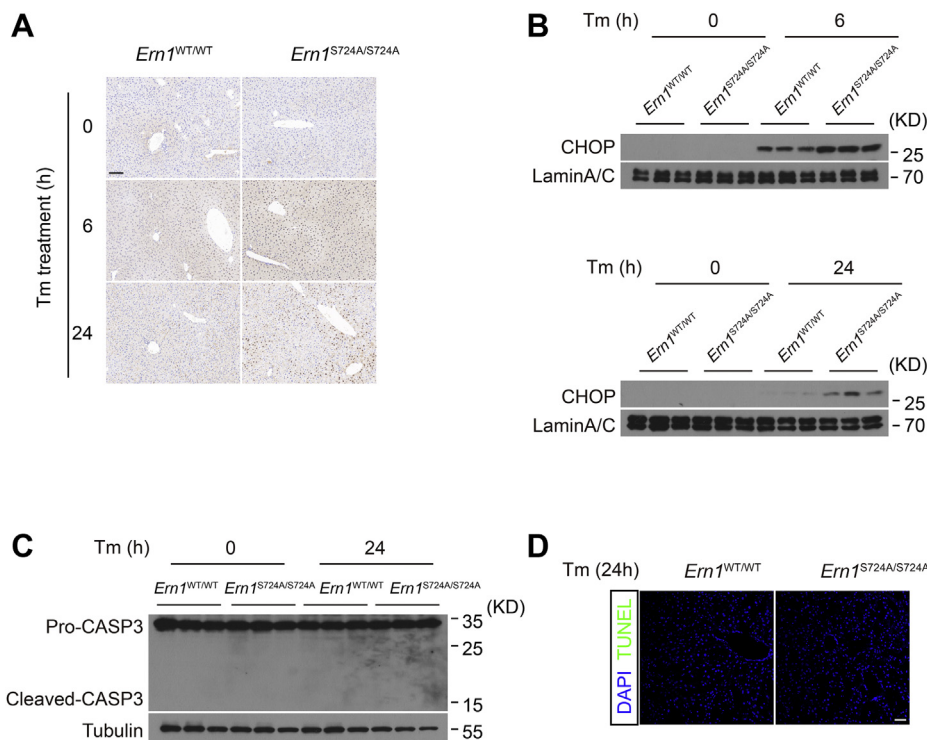


Figure 9. S724A mutation of IRE1 α has no effect upon apoptosis in ER-stressed livers. A, immunohistochemical staining of CHOP protein in liver sections of *Ern1*^{S724A/S724A} mice and their *Ern1*^{WT/WT} littermates following Tm treatment. The scale bar represents 100 μ m. B, immunoblot analysis of CHOP protein in liver nuclear extracts. Lamin A/C was used as the nuclear protein control. C, immunoblot analysis of caspase-3 in livers of mice following Tm treatment for 24 h. Tubulin was used as the loading control. D, representative images of TUNEL staining of liver sections after 24 h of Tm treatment. The scale bar represents 50 μ m. CHOP, CCAAT-enhancer binding protein homologous protein; ER, endoplasmic reticulum; IRE1 α , inositol-requiring enzyme 1 α ; Tm, tunicamycin.

Phosphorylation regulation of IRE1 α activation

mice, we demonstrated *in vivo* that the activation control by phosphorylation at Ser⁷²⁴ of IRE1 α can restrict the severity of ER stress–induced liver steatosis, largely through its RNase-dependent production of XBP1s. Our findings highlight the importance of precisely dissecting the functional consequences *in vivo* of each individual phosphorylation sites or in combinations, which most likely underlies distinct activation modes of IRE1 α under a diversity of stress and pathological conditions.

Phosphorylation at Ser⁷²⁴ has been widely employed for monitoring IRE1 α activation during experimental or physiological ER stress conditions. In contrast to the reported phosphorylation at Ser⁷²⁹ of IRE1 α (38), whose effect upon its kinase activity remains to be characterized, we found that abrogation of Ser⁷²⁴ phosphorylation resulted in decreased or defective autophosphorylation of IRE1 α at certain sites that have yet to be identified. Moreover, these alterations in the phosphorylation state of IRE1 α were subsequently connected to its RNase activities, exhibiting possible cell type–specific features with respect to its RIDD outputs. It is also worth noting that Ser⁷²⁴ of IRE1 α is not only autophosphorylated but also subjected to phosphorylation by PKA kinase in hepatocytes upon glucagon stimulation (55). Thus, it is conceivable that IRE1 α phosphorylation at Ser⁷²⁴ has a key role in governing its activation mode and functional output upon typical ER stress as well as under physiological/pathological stress conditions such as obesity-associated metabolic stress. As IRE1 α is known to be complexed with many other protein partners that either regulate its phosphorylation states or perform downstream signaling functions (32, 56), phosphorylation at Ser⁷²⁴ may represent a key step in controlling the overall phosphorylation states of IRE1 α , which can in turn not only intrinsically regulate its dimerization/oligomerization for activating its RNase activity toward different substrate RNA targets (57) but also modulate its interactions with other proteins for distinct signaling actions. In this context, it warrants further in-depth investigations with regard to potential stress signal–specific mechanisms in eliciting distinct activation modes of IRE1 α through individual or combined phosphorylation events, including those within its kinase activation loop.

Using ER stress–induced hepatic steatosis mouse model, we found that defective activation of IRE1 α as a result of S724A mutation caused deficient production of XBP1s, leading to an exacerbation of lipid accumulation in the liver of Tm-treated *Ern1*^{S724A/S724A} mice. This demonstrates the importance *in vivo* of phosphorylation at Ser⁷²⁴ of IRE1 α for its full activation in counteracting hepatic ER stress, which is consistent with the documented phenotypes in mice with hepatocyte-specific deletion of IRE1 α that abolished *Xbp1* mRNA splicing (51). Mechanistically, a fully functional IRE1 α –XBP1 pathway has been shown to regulate crucial components or regulators of hepatic lipid metabolism, including PDI, PPAR α , and CHOP (43, 50, 54). Particularly, given the reported important role of CHOP in mediating ER stress–induced liver steatosis (54) as well as in transcriptionally suppressing the expression of certain master regulators, for example, *Ppara*, in

hepatic lipid metabolism (58), it is likely that CHOP could act as a key contributor in linking the impaired production of XBP1s in *Ern1*^{S724A/S724A} livers to dysregulated hepatic lipid homeostasis. This is also in line with the reported findings that XBP1s not only downregulates the expression of CHOP (59) but also promotes hepatic lipid secretion through PDI while exerting beneficial metabolic effects upon obesity-associated liver steatosis through suppressing the expression of lipogenic genes (49, 50).

In summary, our study uncovers the functional importance of the phosphorylation at one single serine residue within the kinase activation loop of IRE1 α for its dynamic and endogenous activation in response to ER stress. Because IRE1 α is a multifunctional protein possessing multiple phosphorylation sites, it requires further detailed molecular dissection of the mechanisms that dictate the activation modes of IRE1 α under physiologically and pathologically relevant ER stress conditions such as dietary obesity. This will offer new insights into how dysregulated activation of IRE1 α can link ER stress to the pathogenic development of metabolic disorders such as nonalcoholic fatty liver disease.

Experimental procedures

Animals

All animal studies were conducted in strict accordance with the Institutional Guidelines for the humane treatment of animals, with experimental protocols approved by the Committee on Ethics in the Care and Use of Laboratory Animals, College of Life Sciences, Wuhan University. *Ern1*^{S724A/S724A} knock-in mice were generated by Shanghai Laboratory Animal Co Ltd. For creation of *Ern1*^{S724A/S724A} knock-in mouse model, a pBR322-based targeting vector was generated to contain the segment from 92,210 to 98,830 of the mouse *Ern1* gene (ENSMUSG00000020715) in which the AGT codon for Ser⁷²⁴ residue within exon 17 was substituted with the GCT codon for Ala. Neo cassette flanked by the flippase (FLP) recognition target sequence was then introduced into the targeting sequence between 95,912 and 95,913 of the mouse *Ern1* gene. Targeting vector DNA was used to transfect 129SV/EV (SCR012) embryonic stem (ES) cells by electroporation. After selection with the antibiotic G418, 96 clones were screened by PCR analysis to identify recombinant ES clones, using two sets of primer pairs corresponding to the 5′-homology arm (forward: 5′-CTTCGAGCTACTAGATGGCACTCC-3′), the Neo cassette (reverse: 5′-CCGTGCCTTCCTTGACCCTGG-3′; forward: 5′-GGCCTACCCGCTTCCATTGCTC-3′), and the 3′-homology arm (reverse: 5′-GAAGAACTCACAGCAAA-CATCAG-3′). Two positive clones were identified and then selected for expansion, followed by verification *via* PCR-based DNA sequencing analysis for the presence of the desired AGT to GCT mutation. Targeted ES cells were subsequently microinjected into 194 C57BL/6J blastocysts for 14 recipients, and three male chimeras were obtained and intercrossed with C57BL/6J females to produce F1 heterozygous mice (n = 8). The Neo selection cassette was then removed by breeding to the FLP mice (129S4/SvJaeSor-Gt [ROSA] 26Sortm1 [FLP1]

Dym/J; Jackson Lab), followed by backcrossing of the germline Neo-deleted *Ern1*^{S724A/WT} mice into the genetic background of C57BL/6J for over nine generations. *Ern1*^{S724A/WT} mice were then intercrossed to generate homozygous *Ern1*^{S724A/S724A} mice and *Ern1*^{WT/WT} littermates. Animals were maintained under a standard humidity- and temperature-controlled environment on a 12 h light/dark cycle, with free access to food and water. For ER stress-induced liver steatosis model, 2-month-old male *Ern1*^{S724A/S724A} mice and their *Ern1*^{WT/WT} littermates were injected i.p. with 1 mg/kg body weight of Tm or 150 μ M dextrose (vehicle).

Preparation of MEFs

Primary MEFs were isolated from *Ern1*^{WT/WT} and *Ern1*^{S724A/S724A} embryos at embryonic day 13.5. Briefly, embryos were minced, trypsinized, and washed with PBS. Primary MEFs were plated in Dulbecco's modified Eagle's medium with 10% fetal bovine serum and 1% penicillin–streptomycin. MEFs were then transfected with lentivirus expressing SV40 large T-antigen (kindly provided by Prof Anning Lin at the Shanghai Institutes for Biological Sciences) for immortalization.

Isolation of primary hepatocytes

Primary mouse hepatocytes were isolated from male mice at 8 to 12 weeks of age as previously described (60) with minor modifications. Briefly, collagenase perfusion was performed through the portal vein of anesthetized mice with 50 ml of perfusion buffer (Krebs Ringer buffer containing 3.6 mg/ml glucose, 1 M CaCl₂, and 5000 U of collagenase I [Worthington]) at 37 °C. Cells were dispersed, and hepatocytes were collected and plated in collagen-coated plates with Dulbecco's modified Eagle's medium plus 10% fetal bovine serum. Cells were cultured for 8 h before further analysis.

Serum and liver measurements

Hepatic TGs were measured as previously described (61). Briefly, 20 to 30 mg of liver tissues were homogenized in PBS and mixed with CHCl₃–CH₃OH (2:1, v/v). The organic phase was transferred, air-dried overnight, and resuspended in 1% Triton X-100 in absolute ethanol. Serum and liver TG levels were determined by the Total Triglyceride Kit according to the manufacturer's instructions (Kehua Bioengineering), and liver TG levels were normalized to the total liver protein.

hsSRS imaging

Liver tissue was fixed in 10% formalin and then embedded in Tissue-Tek optimal cutting temperature compound. Frozen liver tissues sectioned to 30 μ m thick using Cryostat (Leica CM 3000) were subjected to hsSRS imaging analysis as previously described (53, 62, 63). Briefly, the spectral focusing-based hsSRS system was used, with a dual-output femtosecond laser (InSight DeepSee; Spectra-Physics) providing pump (800 nm) and Stokes (1040 nm) pulses at an 80 MHz repetition rate. An electro-optical modulator (EO-AM-R-C2; Thorlabs) was used to modulate the Stokes laser at a resonant frequency of 10.5 MHz. The time delay line controlled by a motorized

stage was employed, and the microscope (BX51; Olympus) equipped with a water objective (UPLSAPO 60XW; Olympus) was used for laser scanning and imaging. The pump beam was detected by a photodiode (S3994-01; Hamamatsu) with two installed short-pass filters (ET980SP; Chroma), and the SRS signals were acquired by a lock-in amplifier (HF2 LI; Zurich Instruments). The laser power of pump and Stokes beams were set to 50 and 70 mW (measured before galvanometer), respectively.

Oil-Red O staining

Frozen liver sections (10 μ m thick) were fixed in formalin and then embedded in Tissue-Tek OCT (Servicebio). Liver sections were stained with freshly prepared Oil-Red O solution (Servicebio) for 10 to 30 min, followed by rinsing with 60% isopropanol. Nuclei were lightly stained with alum hematoxylin (Servicebio).

Immunohistochemistry analysis

For immunohistochemical analysis, MEF cells seeded in 96-well PhenoPlates (PerkinElmer; catalog no.: 6055300) at 20,000 cells/well were treated with Tm and fixed with 4% polyformaldehyde for 15 min at room temperature. Cells were then washed twice with PBS and permeabilized with 0.2% Triton X-100 for 7 min at room temperature. After washing with PBS, cells were incubated with blocking buffer (10% fetal bovine serum) for 1 h. After incubation with CHOP antibody (1:100 dilution; Santa Cruz Biotechnology, Inc; catalog no.: sc-7351) overnight at 4 °C, cells were washed three times with PBS, followed by incubation with Alexa Fluor 488–conjugated secondary antibody (1:500 dilution; Invitrogen, catalog no.: A21202) for 1 h at room temperature. Mounting medium was then added before imaging analysis by the Operetta CLS high-content analysis system (PerkinElmer). For liver tissue sections, samples were blocked with 3% bovine serum albumin for 1 h after antigen retrieval and incubation in 3% H₂O₂, followed by incubation with CHOP antibody (1:100 dilution; Santa Cruz Biotechnology, Inc; catalog no.: sc-7351) overnight at 4 °C. After washing with PBS, samples were incubated with horseradish peroxidase–conjugated secondary antibody (1:1000 dilution; Servicebio; catalog no.: GB23303) for 1 h at 37 °C prior to incubation with diaminobenzidine tetrahydrochloride. Images were captured by microscopy.

TUNEL and cell viability analyses

Liver sections were analyzed for cell death using the Dead End Fluorometric TUNEL System (Promega; catalog no.: G3250) according to the manufacturer's instructions. TUNEL signals were visualized by fluorescence microscopy. Cell viability of MEFs and primary hepatocytes was assessed by Enhanced Cell Counting Kit-8 according to the manufacturer's instructions (Beyotime Biotechnology; catalog no.: C0041).

Adenovirus infection

Recombinant adenoviruses for the overexpression of human IRE1 α and its mutant forms, as well as mouse XBP1s, were

Phosphorylation regulation of IRE1 α activation

prepared and used as described previously (44). Primary hepatocytes were infected with adenoviruses at a multiplicity of infection of 20 to 40.

Chemical reagents, antibodies, and immunoblot analysis

Tm (catalog no.: 654380) was purchased from Sigma–Aldrich, and KIRA6 (catalog no.: HY-19708) was from MCE. Antibodies against IRE1 α (catalog no.: 3294), p-PERK (catalog no.: 3179), PERK (catalog no.: 3192), BiP (catalog no.: 3177), ACC1 (catalog no.: 3676), PDI (catalog no.: 3501), and caspase 3 (catalog no.:9662) were all purchased from Cell Signaling Technology. Antibodies against phosphorylated IRE1 α at Ser⁷²⁴ (p-IRE1 α) (catalog no.: AP1146), ADRP (catalog no.: A6276), and CHOP (catalog no.: A0221) were from Abclonal. XBP1s (catalog no.: ab220783) antibody was from Abcam, fatty acid synthase (catalog no.: 610962) antibody was from BD Biosciences, and α -tubulin antibody (T6199) was from Sigma.

For immunoblotting analysis, lysates of liver tissue or cells were prepared by radioimmunoprecipitation assay buffer (150 mM NaCl, 1% NP-40, 0.5% sodium deoxycholate, 0.1% SDS, 50 mM Tris–HCl, pH 7.4) containing cOmplete protease-inhibitor cocktail (Sigma). Protein concentrations were measured by Bradford Protein Assay Kit (Thermo Fisher Scientific). Western immunoblotting was performed as previously described (43), and quantification was done using the ImageJ (National Institutes of Health) software.

Phos-tag gel analysis was performed as described (40). Briefly, a 6% SDS-PAGE gel containing 25 mM Phos-tag was prepared according to the manufacturer's instructions (Phos-tag acrylamide AAL-107; Wako Pure Chemical Industries). IRE1 α antibody (catalog no.: 3294; Cell Signaling Technology) was used to detect the phosphorylated and nonphosphorylated forms of IRE1 α protein.

For preparation of liver nuclear extracts, frozen livers were homogenized using a Dounce homogenizer in ice-cold homogenization buffer I (pH = 8.0) containing 1% NP-40, 10 mM Hepes, 1.5 mM MgCl₂, 10 mM KCl, 25 mM NaF, 1 mM Na₃VO₄, 1 mM EDTA, and cOmplete protease-inhibitor cocktail. The homogenates were briefly centrifuged at 450 rpm at 4 °C to remove tissue debris, and the suspension was transferred to a new tube and centrifuged at 12,000 rpm for 10 min at 4 °C. The nuclear pellets were resuspended in buffer II (pH = 8.0) containing 20 mM Hepes, 1.5 mM MgCl₂, 420 mM NaCl, 0.2 mM EDTA, 25% glycerol, 25 mM NaF, and cOmplete protease-inhibitor cocktail prior to immunoblot analysis using the desired antibodies.

Quantitative RT-PCR analysis

Total RNA was extracted from liver tissue or cells by TRIzol reagent (catalog no.: T9424; Invitrogen), and complementary DNA was synthesized using the RevertAid Synthesis Kit (Thermo Fisher Scientific) according to the manufacturer's instructions. Real-time quantitative PCR was then performed using the ABI Step-one Plus System (Applied Biosystems) with SYBR Green PCR reagents (Applied Biosystems). *Gapdh* was

utilized as the internal control for normalization. The oligonucleotide primers used are as follows:

Mouse *Erdj4*: forward 5'-ATAAAGCCCTGATGCTGAAGC-3' and reverse 5'-GCCATTGGTAAAAGCACTGTGT-3';

Mouse *Xbp1t*: forward 5'-TGGCCGGTCTGCTGAGTCCG-3' and reverse 5'-GTCCATGGGAAGATGTTCTGG-3';

Mouse *Xbp1s*, forward 5'-CTGAGTCCGAATCAGGTG-CAG-3' and reverse 5'-GTCCATGGGAAGATGTTCTGG-3';

Mouse *CHOP*: forward 5'-CTGGAAGCCTGGTATGAGGAT-3' and reverse 5'-CAGGGTCAAGAGTAGTGAAGGT-3';

Mouse *PDI*: forward 5'-ACCTGCTGGTGGAGTTCTATG-3' and reverse 5'-CGGCAGCTTTGGCATACT-3';

Mouse *Bip*: forward 5'-ACTTGGGGACCACCTATTCCT-3' and reverse 5'-ATCGCCAATCAGACGCTCC-3';

Mouse *Gapdh*: forward 5'-GGATTTGGCCGTATTGGG-3' and reverse 5'-GTTGAGGTCAATGAAGGGG-3';

Mouse *Bloc1s1*: forward 5'-TCCCGCCTGCTCAAAGAAC-3' and reverse 5'-GAGGTGATCCACCAACGCTT-3';

Mouse *Ppara*: forward 5'-AGAGCCCCATCTGTCTCTC-3' and reverse 5'-ACTGGTAGTCTGCAAAACCAAA-3';

Mouse *Cpt1a*: forward 5'-CTCCGCCTGAGCCATGAAG-3' and reverse 5'-CACCAGTGATGATGCCATTCT-3';

Mouse *Hmgcs2*: forward 5'-ATATGTGGACCAAACTGACCTGG-3' and reverse 5'-ACTGTTTTGACAGCCTTGGAC-3';

Mouse *Ppar γ* : forward 5'-CTCCAAGAATACCAAAGTGC GA-3' and reverse 5'-GCCTGATGCTTTATCCCCACA-3';

Mouse *Srebp1c*: forward 5'-CAGCTCAGAGCCGTGGT GA-3' and reverse 5'-TTGATAGAAGACCGGTAGCGC-3';

Mouse *Fasn*: forward 5'-GGAGGTGGTGATAGCCGGT AT-3' and reverse 5'-TGGGTAATCCATAGAGCCCAG-3';

Mouse *Acc1*: forward 5'-GATGAACCATCTCCGTTGGC-3' and reverse 5'-CCCAATTATGAATCGGGAGTGC-3';

Mouse *Scd1*: forward 5'-AGATCTCCAGTTCTTACACG ACCAC-3' and reverse 5'-GACGGATGTCTTCTTCCA GGTG-3'.

Mouse *Srebp2*: forward 5'-CCGCTCTCGAATCCTCT-TAT-3' and reverse 5'-CAGCACCTGACTCCAGTGAC-3'.

Statistical analysis

All data are presented as the mean \pm SD. Statistical analysis was conducted using unpaired two-tailed Student's *t* test or two-way ANOVA using GraphPad Prism 7.0 (GraphPad Software, Inc). *p* < 0.05 was considered statistically significant.

Data availability

The data that support the findings of this study are available from the corresponding author upon reasonable request.

Author contributions—Yang Li and Yong Liu conceptualization; Yang Li, J. W., J. D., J. C., and S. H. methodology; S. Y. and P. W. software; Yang Li, S. H., J. W., J. D., J. C., and Z. H. validation; S. Y., P. W., and J. L. formal analysis; Yang Li investigation; Yong Liu resources; Yang Li and S. H. data curation; Yang Li, S. H., and Yong

Liu writing—original draft; Yong Liu writing—review & editing; Yang Li, S. H., and J. W. visualization; P. W. and Yong Liu supervision; Yong Liu project administration; P. W., J. L., and Yong Liu funding acquisition.

Funding and additional information—This work was supported by grants from the National Natural Science Foundation of China (grant nos.: 91857204, 31690102, 32021003, and 91739303; to Yong Liu and J. L.) and the Ministry of Science and Technology of China (National Key R&D Program of China; grant no.: 2018YFA0800700; to Yong Liu). Supported also by Fundamental Research Funds for the Central Universities (grant no.: 2042020kf1056; to Yong Liu). P. W. acknowledges the supports from the National Natural Science Foundation of China (grant no.: 62075076), Science Fund for Creative Research Group of China (grant no.: 61421064), and Innovation Fund of the Wuhan National Laboratory for Optoelectronics.

Conflict of interest—The authors declare that they have no conflicts of interest with the contents of this article.

Abbreviations—The abbreviations used are: ACC1, acetyl-CoA carboxylase 1; *Bip*, binding immunoglobulin protein; CHOP, CCAAT-enhancer binding protein homologous protein; ER, endoplasmic reticulum; ES, embryonic stem; FLP, flippase; hsSRS, hyperspectral stimulated Raman scattering; IRE1, inositol-requiring enzyme 1; MEF, mouse embryonic fibroblast; PDI, protein disulfide isomerase; PERK, PKR-like endoplasmic reticulum kinase; *Ppary*, peroxisome proliferator-activated receptor gamma; RIDD, regulated IRE1-dependent decay; RNase, ribonuclease; *Srebp1*, sterol regulatory element-binding transcription factor 1; Tg, thapsigargin; TG, triacylglyceride; Tm, tunicamycin; UPR, unfolded protein response; XBP-1, X-box binding protein 1; XBP1s, spliced XBP1.

References

- Ron, D., and Walter, P. (2007) Signal integration in the endoplasmic reticulum unfolded protein response. *Nat. Rev. Mol. Cell Biol.* **8**, 519–529
- Walter, P., and Ron, D. (2011) The unfolded protein response: from stress pathway to homeostatic regulation. *Science* **334**, 1081–1086
- Hetz, C., Zhang, K., and Kaufman, R. J. (2020) Mechanisms, regulation and functions of the unfolded protein response. *Nat. Rev. Mol. Cell Biol.* **21**, 421–438
- Hetz, C., and Papa, F. R. (2018) The unfolded protein response and cell fate control. *Mol. Cell* **69**, 169–181
- Wang, M., and Kaufman, R. J. (2016) Protein misfolding in the endoplasmic reticulum as a conduit to human disease. *Nature* **529**, 326–335
- Cubillos-Ruiz, J. R., Bettigole, S. E., and Glimcher, L. H. (2017) Tumorigenic and immunosuppressive effects of endoplasmic reticulum stress in cancer. *Cell* **168**, 692–706
- Hotamisligil, G. S. (2010) Endoplasmic reticulum stress and the inflammatory basis of metabolic disease. *Cell* **140**, 900–917
- Lee, J., and Ozcan, U. (2014) Unfolded protein response signaling and metabolic diseases. *J. Biol. Chem.* **289**, 1203–1211
- Cox, J. S., Shamu, C. E., and Walter, P. (1993) Transcriptional induction of genes encoding endoplasmic reticulum resident proteins requires a transmembrane protein kinase. *Cell* **73**, 1197–1206
- Mori, K., Ma, W., Gething, M. J., and Sambrook, J. (1993) A transmembrane protein with a cdc2+/CDC28-related kinase activity is required for signaling from the ER to the nucleus. *Cell* **74**, 743–756
- Tirasophon, W., Welihinda, A. A., and Kaufman, R. J. (1998) A stress response pathway from the endoplasmic reticulum to the nucleus requires a novel bifunctional protein kinase/endoribonuclease (Ire1p) in mammalian cells. *Genes Dev.* **12**, 1812–1824
- Credle, J. J., Finer-Moore, J. S., Papa, F. R., Stroud, R. M., and Walter, P. (2005) On the mechanism of sensing unfolded protein in the endoplasmic reticulum. *Proc. Natl. Acad. Sci. U. S. A.* **102**, 18773–18784
- Sidrauski, C., and Walter, P. (1997) The transmembrane kinase Ire1p is a site-specific endonuclease that initiates mRNA splicing in the unfolded protein response. *Cell* **90**, 1031–1039
- Hetz, C., Martinon, F., Rodriguez, D., and Glimcher, L. H. (2011) The unfolded protein response: integrating stress signals through the stress sensor IRE1alpha. *Physiol. Rev.* **91**, 1219–1243
- Zhou, J., Liu, C. Y., Back, S. H., Clark, R. L., Peisach, D., Xu, Z., et al. (2006) The crystal structure of human IRE1 luminal domain reveals a conserved dimerization interface required for activation of the unfolded protein response. *Proc. Natl. Acad. Sci. U. S. A.* **103**, 14343–14348
- Lee, K. P., Dey, M., Neculai, D., Cao, C., Dever, T. E., and Sicheri, F. (2008) Structure of the dual enzyme Ire1 reveals the basis for catalysis and regulation in nonconventional RNA splicing. *Cell* **132**, 89–100
- Korennykh, A. V., Egea, P. F., Korostelev, A. A., Finer-Moore, J., Zhang, C., Shokat, K. M., et al. (2009) The unfolded protein response signals through high-order assembly of Ire1. *Nature* **457**, 687–693
- Ali, M. M., Bagratuni, T., Davenport, E. L., Nowak, P. R., Silva-Santesteban, M. C., Hardcastle, A., et al. (2011) Structure of the Ire1 autophosphorylation complex and implications for the unfolded protein response. *EMBO J.* **30**, 894–905
- Shen, X., Ellis, R. E., Lee, K., Liu, C. Y., Yang, K., Solomon, A., et al. (2001) Complementary signaling pathways regulate the unfolded protein response and are required for *C. elegans* development. *Cell* **107**, 893–903
- Yoshida, H., Matsui, T., Yamamoto, A., Okada, T., and Mori, K. (2001) XBP1 mRNA is induced by ATF6 and spliced by IRE1 in response to ER stress to produce a highly active transcription factor. *Cell* **107**, 881–891
- Calfon, M., Zeng, H., Urano, F., Till, J. H., Hubbard, S. R., Harding, H. P., et al. (2002) IRE1 couples endoplasmic reticulum load to secretory capacity by processing the XBP-1 mRNA. *Nature* **415**, 92–96
- Han, J., and Kaufman, R. J. (2017) Physiological/pathological ramifications of transcription factors in the unfolded protein response. *Genes Dev.* **31**, 1417–1438
- Vembar, S. S., and Brodsky, J. L. (2008) One step at a time: endoplasmic reticulum-associated degradation. *Nat. Rev. Mol. Cell Biol.* **9**, 944–957
- Ruggiano, A., Foresti, O., and Carvalho, P. (2014) Quality control: ER-associated degradation: protein quality control and beyond. *J. Cell Biol.* **204**, 869–879
- Hwang, J., and Qi, L. (2018) Quality control in the endoplasmic reticulum: crosstalk between ERAD and UPR pathways. *Trends Biochem. Sci.* **43**, 593–605
- Hollien, J., and Weissman, J. S. (2006) Decay of endoplasmic reticulum-localized mRNAs during the unfolded protein response. *Science* **313**, 104–107
- Hollien, J., Lin, J. H., Li, H., Stevens, N., Walter, P., and Weissman, J. S. (2009) Regulated Ire1-dependent decay of messenger RNAs in mammalian cells. *J. Cell Biol.* **186**, 323–331
- Maurel, M., Chevet, E., Tavernier, J., and Gerlo, S. (2014) Getting RIDD of RNA: IRE1 in cell fate regulation. *Trends Biochem. Sci.* **39**, 245–254
- Upton, J. P., Wang, L., Han, D., Wang, E. S., Huskey, N. E., Lim, L., et al. (2012) IRE1alpha cleaves select microRNAs during ER stress to derepress translation of proapoptotic Caspase-2. *Science* **338**, 818–822
- Wang, J. M., Qiu, Y., Yang, Z. Q., Li, L., and Zhang, K. (2017) Inositol-requiring enzyme 1 facilitates diabetic wound healing through modulating microRNAs. *Diabetes* **66**, 177–192
- Sha, H., He, Y., Yang, L., and Qi, L. (2011) Stressed out about obesity: IRE1alpha-XBP1 in metabolic disorders. *Trends Endocrinol. Metab.* **22**, 374–381
- Huang, S., Xing, Y., and Liu, Y. (2019) Emerging roles for the ER stress sensor IRE1alpha in metabolic regulation and disease. *J. Biol. Chem.* **294**, 18726–18741
- Shamu, C. E., and Walter, P. (1996) Oligomerization and phosphorylation of the Ire1p kinase during intracellular signaling from the endoplasmic reticulum to the nucleus. *EMBO J.* **15**, 3028–3039
- Welihinda, A. A., and Kaufman, R. J. (1996) The unfolded protein response pathway in *Saccharomyces cerevisiae*. Oligomerization and trans-phosphorylation of Ire1p are required for kinase activation. *J. Biol. Chem.* **271**, 18181–18187

Phosphorylation regulation of IRE1 α activation

35. Tirasophon, W., Lee, K., Callaghan, B., Welihinda, A., and Kaufman, R. J. (2000) The endoribonuclease activity of mammalian IRE1 autoregulates its mRNA and is required for the unfolded protein response. *Genes Dev.* **14**, 2725–2736
36. Prisch, F., Nowak, P. R., Carrara, M., and Ali, M. M. (2014) Phosphoregulation of Ire1 RNase splicing activity. *Nat. Commun.* **5**, 3554
37. Chang, T. K., Lawrence, D. A., Lu, M., Tan, J., Harnoss, J. M., Marsters, S. A., *et al.* (2018) Coordination between two branches of the unfolded protein response determines apoptotic cell fate. *Mol. Cell* **71**, 629–636.e5
38. Tang, C. H., Chang, S., Paton, A. W., Paton, J. C., Gabrilovich, D. I., Ploegh, H. L., *et al.* (2018) Phosphorylation of IRE1 at S729 regulates RIDD in B cells and antibody production after immunization. *J. Cell Biol.* **217**, 1739–1755
39. Yang, L., Xue, Z., He, Y., Sun, S., Chen, H., and Qi, L. (2010) A Phos-tag-based approach reveals the extent of physiological endoplasmic reticulum stress. *PLoS One* **5**, e11621
40. Qi, L., Yang, L., and Chen, H. (2011) Detecting and quantitating physiological endoplasmic reticulum stress. *Methods Enzymol.* **490**, 137–146
41. Ghosh, R., Wang, L., Wang, E. S., Perera, B. G., Igarria, A., Morita, S., *et al.* (2014) Allosteric inhibition of the IRE1 α RNase preserves cell viability and function during endoplasmic reticulum stress. *Cell* **158**, 534–548
42. Bae, D., Moore, K. A., Mella, J. M., Hayashi, S. Y., and Hollien, J. (2019) Degradation of Blos1 mRNA by IRE1 repositions lysosomes and protects cells from stress. *J. Cell Biol.* **218**, 1118–1127
43. Shao, M., Shan, B., Liu, Y., Deng, Y., Yan, C., Wu, Y., *et al.* (2014) Hepatic IRE1 α regulates fasting-induced metabolic adaptive programs through the XBP1s-PPAR α axis signalling. *Nat. Commun.* **5**, 3528
44. Qiu, Y., Mao, T., Zhang, Y., Shao, M., You, J., Ding, Q., *et al.* (2010) A crucial role for RACK1 in the regulation of glucose-stimulated IRE1 α activation in pancreatic beta cells. *Sci. Signal.* **3**, ra7
45. Baiceanu, A., Mesdom, P., Lagouge, M., and Foulle, F. (2016) Endoplasmic reticulum proteostasis in hepatic steatosis. *Nat. Rev. Endocrinol.* **12**, 710–722
46. Lebeaupin, C., Vallee, D., Hazari, Y., Hetz, C., Chevet, E., and Bailly-Maitre, B. (2018) Endoplasmic reticulum stress signalling and the pathogenesis of non-alcoholic fatty liver disease. *J. Hepatol.* **69**, 927–947
47. Song, M. J., and Malhi, H. (2019) The unfolded protein response and hepatic lipid metabolism in non alcoholic fatty liver disease. *Pharmacol. Ther.* **203**, 107401
48. Lee, A. H., Scapa, E. F., Cohen, D. E., and Glimcher, L. H. (2008) Regulation of hepatic lipogenesis by the transcription factor XBP1. *Science* **320**, 1492–1496
49. Herrema, H., Zhou, Y., Zhang, D., Lee, J., Salazar Hernandez, M. A., Shulman, G. I., *et al.* (2016) XBP1s is an anti-lipogenic protein. *J. Biol. Chem.* **291**, 17394–17404
50. Wang, S., Chen, Z., Lam, V., Han, J., Hassler, J., Finck, B. N., *et al.* (2012) IRE1 α -XBP1s induces PDI expression to increase MTP activity for hepatic VLDL assembly and lipid homeostasis. *Cell Metab.* **16**, 473–486
51. Zhang, K., Wang, S., Malhotra, J., Hassler, J. R., Back, S. H., Wang, G., *et al.* (2011) The unfolded protein response transducer IRE1 α prevents ER stress-induced hepatic steatosis. *EMBO J.* **30**, 1357–1375
52. Jiang, S., Yan, C., Fang, Q. C., Shao, M. L., Zhang, Y. L., Liu, Y., *et al.* (2014) Fibroblast growth factor 21 is regulated by the IRE1 α -XBP1 branch of the unfolded protein response and counteracts endoplasmic reticulum stress-induced hepatic steatosis. *J. Biol. Chem.* **289**, 29751–29765
53. Fu, D., Yu, Y., Folick, A., Currie, E., Farese, R. V., Jr., Tsai, T. H., *et al.* (2014) *In vivo* metabolic fingerprinting of neutral lipids with hyperspectral stimulated Raman scattering microscopy. *J. Am. Chem. Soc.* **136**, 8820–8828
54. Rutkowski, D. T., Wu, J., Back, S. H., Callaghan, M. U., Ferris, S. P., Iqbal, J., *et al.* (2008) UPR pathways combine to prevent hepatic steatosis caused by ER stress-mediated suppression of transcriptional master regulators. *Dev. Cell* **15**, 829–840
55. Mao, T., Shao, M., Qiu, Y., Huang, J., Zhang, Y., Song, B., *et al.* (2011) PKA phosphorylation couples hepatic inositol-requiring enzyme 1 α to glucagon signaling in glucose metabolism. *Proc. Natl. Acad. Sci. U. S. A.* **108**, 15852–15857
56. Hetz, C., and Glimcher, L. H. (2009) Fine-tuning of the unfolded protein response: assembling the IRE1 α interactome. *Mol. Cell* **35**, 551–561
57. Le Thomas, A., Ferri, E., Marsters, S., Harnoss, J. M., Lawrence, D. A., Zuazo-Gatzelu, I., *et al.* (2021) Decoding non-canonical mRNA decay by the endoplasmic-reticulum stress sensor IRE1 α . *Nat. Commun.* **12**, 7310
58. Chikka, M. R., McCabe, D. D., Tyra, H. M., and Rutkowski, D. T. (2013) C/EBP homologous protein (CHOP) contributes to suppression of metabolic genes during endoplasmic reticulum stress in the liver. *J. Biol. Chem.* **288**, 4405–4415
59. Huang, C., Wang, J. J., Ma, J. H., Jin, C., Yu, Q., and Zhang, S. X. (2015) Activation of the UPR protects against cigarette smoke-induced RPE apoptosis through up-regulation of Nrf2. *J. Biol. Chem.* **290**, 5367–5380
60. Wang, Q., Jiang, L., Wang, J., Li, S., Yu, Y., You, J., *et al.* (2009) Abrogation of hepatic ATP-citrate lyase protects against fatty liver and ameliorates hyperglycemia in leptin receptor-deficient mice. *Hepatology* **49**, 1166–1175
61. Liu, Y., Shao, M., Wu, Y., Yan, C., Jiang, S., Liu, J., *et al.* (2015) Role for the endoplasmic reticulum stress sensor IRE1 α in liver regenerative responses. *J. Hepatol.* **62**, 590–598
62. Tian, S., Li, H., Li, Z., Tang, H., Yin, M., Chen, Y., *et al.* (2020) Polydiacetylene-based ultrastrong bioorthogonal Raman probes for targeted live-cell Raman imaging. *Nat. Commun.* **11**, 81
63. Huang, B., Yan, S., Xiao, L., Ji, R., Yang, L., Miao, A. J., *et al.* (2018) Label-free imaging of nanoparticle uptake competition in single cells by hyperspectral stimulated Raman scattering. *Small* **14**. <https://doi.org/10.1002/sml.201703246>